Journal of Hydrology: Regional Studies 61 (2025) 102751

Contents lists available at ScienceDirect

Journal of Hydrology: Regional Studies

journal homepage: www.elsevier.com/locate/ejrh

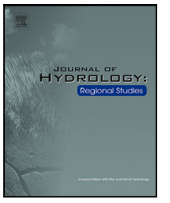

Comparative analysis of land–atmosphere interactions across three contrasting ecosystems in the West Sudanian Savanna

Luitpold Hingerl [a,c,*], Jan Bliefernicht [a], Samuel Guug [b], Souleymane Sy [a], Frank Neidl [c], Thomas Jagdhuber [a,d], Harald Kunstmann [a,c]

[a] Institute of Geography, University of Augsburg, Augsburg, Germany
[b] WASCAL Competence Center, West African Science Service Center on Climate Change and Adapted Land Use, Ouagadougou, Burkina Faso
[c] Institute for Meteorology and Climate Research, Campus Alpin, Karlsruhe Institute of Technology, Garmisch-Partenkirchen, Germany
[d] Microwaves and Radar Institute, German Aerospace Center (DLR), Wessling, Germany

ARTICLE INFO

Keywords:
Land atmosphere coupling
Energy partitioning
Eddy covariance measurements
Water- and energy fluxes
West Africa

ABSTRACT

Study region: The Sudanian Savanna in northern Ghana and southern Burkina Faso is undergoing extensive land use change due to rapid population growth, altering surface–atmosphere interactions and regional climate dynamics.

Study focus: Limited data availability hampers observation-based assessments of land use change (LUC) impacts. To address this, we conducted a multi-year analysis of energy fluxes and land–atmosphere coupling using eddy covariance (EC) data from three contrasting ecosystems: near-natural savanna, cropland, and degraded grassland. We examined energy balance partitioning and derived surface parameters such as surface conductance. Despite similar climate and soil conditions, the near-natural savanna exhibited 30% higher net radiation and nearly half the albedo (0.16) of the degraded grassland (0.29). Evaporative fraction (EF) at agricultural sites was up to 30% lower during the dry season and monsoon transitions. Partial correlation analysis identified leaf area index (LAI) and upper soil moisture as key drivers of these differences, with EF most sensitive to LAI at the degraded grassland ($r = 0.54$) and least sensitive to soil moisture at the savanna site ($r = 0.23$). These results underline the complexity of LAI dynamics across ecosystems, particularly given uncertainties in tree phenology and variable tree cover.

New hydrometeorological insights for the region: Land–atmosphere coupling remained consistent across the three ecosystems during most WAM seasons but differed markedly during the drying phase. The results highlight the role of land cover in shaping surface fluxes and underscore the importance of long-term flux observations to understand LUC impacts on regional climate and hydrology.

1. Introduction

The West African Sudanian Savanna region is currently experiencing significant land use changes mainly driven by population growth, agricultural expansion and urbanization (Potapov et al., 2022; Bliefernicht et al., 2018; Flörke et al., 2018; Neupane and Kumar, 2015; Waller et al., 2007; Xue, 2017). These anthropogenic changes can have significant impacts on land–atmosphere processes and interactions, affecting the climate at both local and regional scales (Sy et al., 2017; Snyder et al., 2004; Mortey et al., 2023; Boone et al., 2016). The need to comprehend these dynamics is particularly crucial given that West Africa has been

* Corresponding author at: Institute for Meteorology and Climate Research, Campus Alpin, Karlsruhe Institute of Technology, Garmisch-Partenkirchen, Germany.
E-mail address: luitpold.hingerl@kit.edu (L. Hingerl).

https://doi.org/10.1016/j.ejrh.2025.102751
Received 7 March 2025; Received in revised form 27 August 2025; Accepted 28 August 2025
Available online 9 September 2025

identified as a global hotspot for land–atmosphere interactions. This designation is based on findings by Koster et al. (2004, 2006), who used the GLACE modeling comparison experiment to identify regions with the strongest land–atmosphere coupling. Therefore, analyzing the impacts of land use changes and resulting shifts in land–atmosphere interactions is also essential for assessing future climate changes (Wulfmeyer et al., 2014; Harper et al., 2018; Späth et al., 2023; Duveiller et al., 2020; Sy and Quesada, 2020; Arnault et al., 2023; Ndiaye et al., 2024; Röll et al., 2019). For example in modeling studies enhancing the representation of land–atmosphere exchange processes and their feedback mechanisms is vital for gaining deeper insights into human impacts on the environment and climate (Sy et al., 2017; Sy and Quesada, 2020). Specifically land surface characteristics such as albedo, surface roughness and soil moisture have been highlighted in several studies as having a strong connection with atmospheric processes (Xue, 2017; Xue et al., 2012; Koster et al., 2004, 2006; Seneviratne et al., 2010). However, land–atmosphere interactions and their underlying physical mechanics remain largely unexplored, particularly in data-scarce regions like the West African Sudanian Savanna. This is primarily due to the lack of sufficient observational infrastructure for in-situ measurements, which limits the ability to observe and analyze these processes in detail (e.g., Lorenz and Kunstmann, 2012; Salack et al., 2019; Bliefernicht et al., 2022).

For a better understanding of land surface processes and interactions, observational studies based on micro-meteorological equipment, such as eddy covariance stations, are nowadays widely used (Nadolski et al., 2024; Bliefernicht et al., 2018; Widmoser and Wohlfahrt, 2018). Early experiments of this kind were carried out in West Africa through various field campaigns over the past decades and have provided important insights into land–atmosphere interactions. The SEBEX experiment (Wallace et al., 1991; Kahan et al., 2006) examined how different land cover types affect seasonal energy fluxes. HAPEX-Sahel (Goutorbe et al., 1994) combined multi-scale observations and modeling to improve land surface parameterizations for semi-arid regions. NIMEX-1 (Jegede et al., 2004) focused on energy balance components under wet and dry tropical conditions in southwestern Nigeria. AMMA-CATCH (Lebel et al., 2009; Galle et al., 2018) linked flux responses to rainfall variability and vegetation phenology, emphasizing land use impacts on water resource management (Allies et al., 2022; Rahimi et al., 2021; Verbruggen et al., 2020; Merk et al., 2024; Hounsinou et al., 2022). Mamadou et al. (2014, 2016) highlighted strong seasonal contrasts in fluxes and identified soil moisture as the main control on energy partitioning. Additional studies using scintillometers confirmed the complexity of flux dynamics in heterogeneous landscapes (Guyot et al., 2012; Hssaine et al., 2018). However, important knowledge gaps remain, particularly concerning the long-term effects of land use change on land–atmosphere interactions and their implications for local and regional climate and hydrology. Extended observational time series are needed to capture interannual variability and to better understand how different land management practices influence surface fluxes and atmospheric feedbacks. Moreover, additional ecosystem types should be included to comprehensively assess the diversity of land surface responses across the region.

In 2012, a unique micro-meteorological experiment was established in West Africa as part of the WASCAL (West African Science Service Center on Climate Change and Adapted Land Use) observatory (Bliefernicht et al., 2013, 2018; Salack et al., 2019; Nadolski et al., 2024). The land use of the study region is highly heterogeneous due to significant land use changes in the past (Bliefernicht et al., 2018). As most people in Burkina Faso and Ghana rely on subsistence agriculture, tremendous population growth has led to a substantial increase in farmland in this region (Knauer et al., 2016). Hence the goal of the WASCAL observatory is to analyze the impact of land use changes on water, energy and CO_2 fluxes in contrasting land use sites in the West African Sudanian savanna in a long term manner (Nadolski et al., 2024). To realize this task, different ecosystem sites (e.g. near natural savanna, cropland, degraded grassland) were equipped with EC devices. Over the last 13 years a series of studies was published using the measurement data of these sites. For instance, Quansah et al. (2015) analyzed the CO_2 fluxes from three contrasting sites using one-year measurement data. The studies showed that CO_2 uptake was highest during the rainy season. The near natural vegetation acts as a CO_2 sink due to larger CO_2 uptake and water use efficiency. Across the last decade, the EC setup could successfully be used to answer questions on rain induced CO_2 emissions (Berger et al., 2019) and seasonal variation of systematic errors in the estimation of energy balance components (Nadolski et al., 2024). However, a detailed analysis of the individual land–atmosphere processes is still lacking, despite their crucial role in linking surface conditions with atmospheric dynamics.

This study aims to close this gap by investigating the effects of land use change on land–atmosphere processes and interactions across three contrasting ecosystems (near natural savanna, cropland, and grassland) in the Sudanian savanna of West Africa. The following three key scientific questions will be addressed: (1) How do different land use types at the three sites affect the radiative properties and the partitioning of energy fluxes under similar climatic conditions? (2) What are the potential drivers of the spatiotemporal variability in land–atmosphere interactions? (3) How do different land use types affect land–atmosphere coupling properties? Unlike previous studies conducted in this region (e.g., Quansah et al., 2015; Mamadou et al., 2016; Berger et al., 2019; Nadolski et al., 2024) this research presents, for the first time, a detailed analysis of energy fluxes and radiation components across all three ecosystems over a three-year period, which was chosen for its exceptionally high data consistency and quality.

2. Study region and site characteristics

The selected EC sites of the WASCAL observatory are located close to the Ghanaian-Burkinabe border along a transect of changing land use. They are located at three contrasting ecosystems and land use sites (near natural savanna, cropland, degraded grassland) as shown in Fig. 1. The near natural savanna site is situated in the Nazinga Park within a research field in the core protection zone of the park (Bliefernicht et al., 2018). This site represents a near-natural Sudanian savanna ecosystem with no agricultural management activities. We refer to it as “near-natural” instead of “pure-natural”, as some degree of anthropogenic influence on the vegetation cannot be entirely ruled out, given the historically dense population in the area. The vegetation at this site is a mixture of grass, trees, and bushes (Berger et al., 2019). During the rainy season, grass can reach a height of up to 2.5 meters (Table 1).

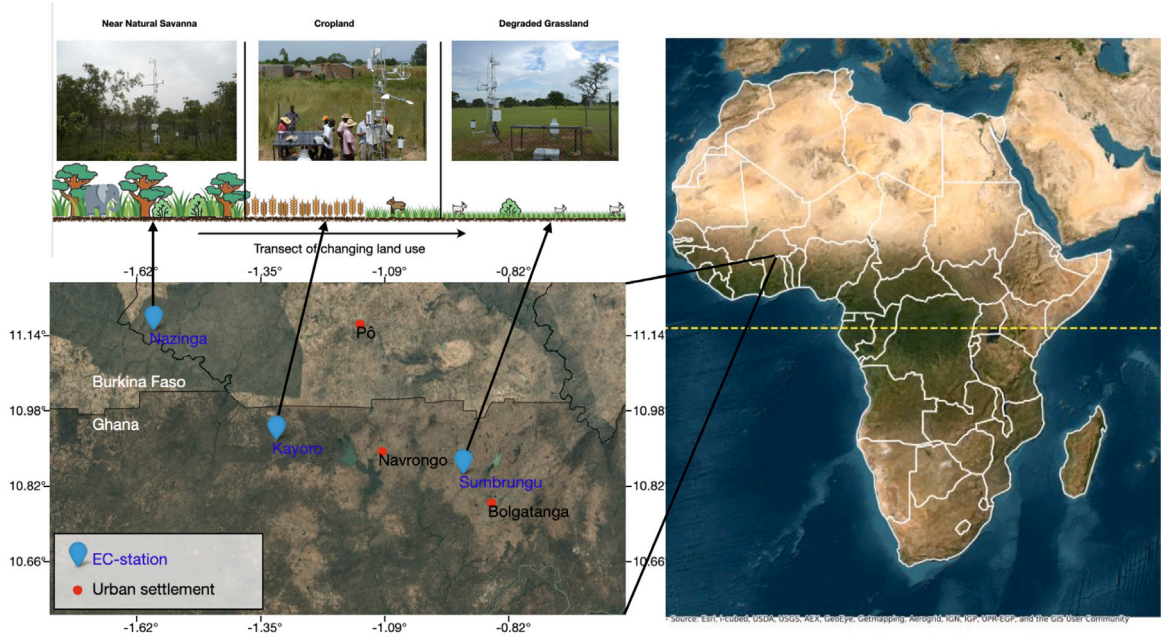

Fig. 1. The location of the selected eddy covariance stations. Nazinga represents the near natural savanna ecosystem, Kayoro is characterized by cropland, and Sumbrungu is located in a degraded grassland area. The red dots represent urban settlements, with Bolgatanga and Navrongo located in northern Ghana, while Po is situated in southern Burkina Faso. The experimental setup includes a schematic representation of the transect, highlighting variations in land use and land management changes, accompanied by images showing the different ecosystem types surrounding the three eddy covariance (EC) stations. The EC stations belong to the mesoscale observatory operated by WASCAL and its partner institutions in this region since 2013 (Bliefernicht et al., 2018, Salack et al., 2019).

The mean height of trees in the surrounding area ranges from 4 to 5 meters (Table 1), with the tallest trees reaching 8 to 10 meters (Bliefernicht et al., 2018). With a coverage of about 28%, the density of trees and bushes is considerably higher compared to the degraded grassland site. The soil texture is similar to the one of the degraded grassland site but has a higher clay content. Additionally, the soil organic carbon level, measured at 3.3%, is the highest among the sites (Table 1).

The degraded grassland site is situated in Sumbrungu northwest of Bolgatanga in northern Ghana. This site represents a highly degraded area with intensive agricultural management. Crop cultivation is nowadays found only at foot slope positions in this area (Berger et al., 2019). The immediate surroundings of the EC station (< 200 m) are predominantly used as rangeland for livestock (Berger et al., 2019) the year round with a stocking rate between 6–8 animals per hectare (Quansah et al., 2015) leading to the maximum grass height of 10 cm. The area directly around the EC station is interspersed with individual trees and bushes, averaging about 5 m in height, with an approximate distance of 50 m between them (Bliefernicht et al., 2018) and a coverage of about 3% of the study area. A picture of the EC station during the wet-to-dry transitional period and its surrounding vegetation is shown in Fig. 1 (degraded grassland). The soil at the EC site is degraded but contains with 1.6% of total soil mass still a considerable amount of organic carbon in the topsoil (Table 1). The soil texture is loamy sand with a high proportion of coarse-grained materials, extending to a depth of 50 cm (Bliefernicht et al., 2018).

The cropland site is located between the grassland and near-nature sites in a less populated area that is partially used for agriculture. This site is situated near the small village of Kayoro. The surrounding area of the EC station is alternately used for tillage agriculture and fallow. During fallow periods, the mean maximum grass height is around one meter (Table 1). In periods when the area is used for tillage, as it was the case during the three years of this study, groundnut plants, which reach an average height of about 30 cm, cover the surroundings of the EC station almost homogeneously. The soil texture is very similar to that of the previous sites, but differs in its chemical properties, having with 0.62% a smaller proportion of organic carbon in the topsoil (Table 1). The terrain of this EC site is flat, consistent with the topography observed at all other EC sites.

It is important to note that the degraded grassland site experienced severe vandalism in 2016, necessitating its relocation and disrupting subsequent measurements (Bliefernicht et al., 2022). Consequently, this study, similar to the recent study by Nadolski et al. (2024), focuses on a unique measurement period (2013–2015), chosen for its high data availability and consistency. In addition to the EC data, satellite-derived Leaf Area Index (LAI) from the MOD15A2H version 6 data with 500 m spatial resolution (Myneni et al., 2015) is used.

3. Statistical analysis and derived quantities

The applied statistical methods and derived quantities in this study are carried out in the following order: First, a detailed analysis of the energy balance components is performed for the different monsoon seasons. Next, potential drivers of the altered

Table 1
Basic climate, land use and soil characteristics of the selected savanna sites (near natural savanna, cropland, and degraded grassland) (Bliefernicht et al., 2018; Berger et al., 2019).

Characteristic	Near natural savanna	Cropland	Degraded grassland
Latitude, °N	11.1556	10.91810	10.84660
Longitude, °W	−1.58570	−1.32900	−0.91700
Altitude [m a.s.l.]	293	292	200
Mean annual precipitation [mm]	994	960	978
Mean annual temperature [°C]	28.6	29.2	28.3
Land use	Protected area	Cropland	Grassland
Land use intensity	Very low	High	High
Max. grass height [m]	2.5	1	0.1
Tree coverage [%]	27	<1	3
Mean tree height [m]	4.5	5	5
Relief	Flat	Flat	Flat
Soil texture	Sandy loam	Loamy sand	Loamy sand
Soil organic carbon content [mass-%]	3.30	0.62	1.60
Soil mineral content [mass-%]	50.30	52.84	51.74

land–atmosphere interactions are identified for the study area. As a third step, key surface parameters, such as surface conductance, are calculated for the different EC sites and monsoonal periods, which are critical for land–atmosphere coupling. Lastly, a footprint analysis is conducted to determine the footprint of the EC measurements. In the following sections, a detailed description of the statistical analysis is provided. We focus on the calculation of surface parameters and the footprint analysis, as these are the most complex aspects of our study.

3.1. Eddy covariance data processing and heat flux estimation

To assess turbulent energy fluxes, we employ a sonic anemometer (CSAT3, Campbell) to measure the three-dimensional wind field, an infrared open path gas analyzer (7500 A, Li-COR) to determine air water content and CO_2 concentration, and a thermometer to monitor air temperature. These measurements are taken at a frequency of 20 Hz. The resulting high-frequency data is processed automatically by a field computer integrated into the logger system, utilizing the statistical software package TK3 (Mauder and Foken, 2011; Fratini and Mauder, 2014; Mauder and Foken, 2015; Soltani et al., 2018; Lan et al., 2024; Paulus et al., 2024), which includes a variety of statistical correction techniques for a refinement of the measurements. For example a set of spectral correction is carried out in TK3 like high frequency loss due to path length averaging of vectors and scalars, high frequency loss due to spatial separation of sensors, high frequency loss due to frequency dynamic response and high frequency loss due to electronic filtering. In addition low frequency spectral corrections like the spectral models for stable stratification after Moore (1986) and for unstable stratification after Højstrup (1981) are applied. At the end of each 30 min measurement interval, the system carries out plausibility tests, calculates the average of the measured variables and their variance and covariance. This process enables the on-site determination of sensible heat flux H $\left(\mathrm{W\,m^{-2}}\right)$, latent heat flux LE $\left(\mathrm{W\,m^{-2}}\right)$, and net ecosystem exchange. Additionally, the TK3 software package carries out quality tests to ensure the reliability of the data. Based on these tests, all measurements in the time series are marked with a flag, and any data flagged as having insufficient reliability were excluded from this analysis. We used the flags after the Spoleto agreement in our setup (Mauder et al., 2013) with the flag 0 indicating high quality, 1 moderate quality and 2 low quality data. Data with the flag 2 have been filtered out (see A.5 for a comparison of filtered and unfiltered amounts of data). For more details about these quality tests please refer to Mauder and Foken (2015). The energy balance closure of the three EC stations was analyzed by Quansah et al. (2015) and Nadolski et al. (2024). Their calculated values of 0.89 for the near natural savanna, 0.67 for cropland and 0.67 for the degraded grassland indicate sufficient data quality. In addition, a number of further variables are calculated on site such as the net total radiation and the surface scattering albedo using the measurements from the CNR4 net radiometer (Blonquist Jr. et al., 2009). The temporal resolution of the radiation variables is 5 min.

In this study the delineation of the four monsoon seasons was carried out using a criterion based on the measured absolute humidity of the air q_a $\left(\mathrm{g/m^3}\right)$, since q_a was measured directly at all sites with a gas analyzer (7500 A, Li-COR). Mamadou et al. (2014) confirmed the accuracy of this method by comparing it to the zonal wind and water vapor mixing ratio (WVMR) approach as proposed by Sultan and Janicot (2003) and Lothon et al. (2008) to delineate the seasons. The rainy season was defined when q_a exceeded 16 $\mathrm{g/m^3}$ for a minimum of 5 days. Conversely, the dry season was identified when the criterion of q_a less than 6 $\mathrm{g/m^3}$ was met for a minimum of 5 days. Transitional periods were defined when neither of these criteria were met.

To obtain a consistent assessment of peak solar conditions, midday averages were calculated for the period between 10:00 and 14:00 local time every day. For the diurnal cycles of the measured turbulent fluxes, the half-hourly data were averaged over the defined midday period during the specified four seasons, ensuring a representation of seasonal variations. To facilitate better comparability of the energy partitioning between the stations, we calculated the evaporative fraction (EF) using the midday means as:

$$EF = \frac{LE}{LE + H} \tag{1}$$

where LE is the latent and H the sensible heat flux (W m^{-2}). Note that the flux data shown in Fig. 6 were gap-filled using the REddyProc package for R (Wutzler et al., 2018) to enable better visual comparison. All other analyses in the manuscript were conducted exclusively using observed (non-gap-filled) data.

3.2. Interpolation and gap filling methods for the hydrological analysis

To enable a hydrological analysis, gap filling methods were applied to the meteorological variables and ET. First, to address 20%–30% data gaps in the original EC station time series, meteorological data from nearby weather stations were used for gap-filling. A nearest-neighbor approach was applied, using data from the closest station, followed by the second closest if gaps remained. Afterward, outliers and implausible values (e.g. $RH > 100\%$, extreme wind speeds) were removed. Remaining gaps (5%–10%) were filled via linear interpolation for gaps < 4 h and a diurnal-mean method for longer gaps (> 4 h), preserving diurnal variability.

Second, gaps in the ET time series were filled using simulation results from the NOAH land surface model (version 3.4.1., Ek et al. 2003). This approach was chosen because NOAH provides physically consistent estimates of land–atmosphere fluxes, ensuring that gap-filled ET values remain constrained by meteorological drivers and surface characteristics.

3.3. Calculation of surface parameters

For the calculation of surface parameters the R Bigleafe package (Knauer et al., 2018) was used. The ability of the surface to transport heat and water vapor from the surface to the atmosphere can be expressed with the aerodynamic conductance G_a $(\mathrm{m\ s^{-1}})$:

$$G_a = \frac{1}{(R_{am} + R_{bh})} \tag{2}$$

where R_{am} is the aerodynamic resistance to momentum and is calculated as:

$$R_{am} = \frac{u}{u_*^2} \tag{3}$$

u represents the measured wind speed (m s^{-1}) and u_* denotes the friction velocity (m s^{-1}). In this formulation atmospheric stability is inherently accounted for by u_* as a measure of turbulent momentum transfer near the surface. This approach eliminates the need for additional stability correction functions.

R_{bh} represents the canopy boundary layer resistance to heat transfer, which is primarily governed by molecular diffusion as the main transport mechanism, and is calculated after Thom (1972) as:

$$R_{bh} = 6.2u_*^{-0.667} \tag{4}$$

The surface conductance G_s $(\mathrm{m\ s^{-1}})$ is calculated using the inverted Penman-Monteith equation (Penman, 1948) as follows:

$$G_s = \frac{LE \cdot G_a \cdot \gamma}{\Delta \cdot A + \rho \cdot c_p \cdot G_a \cdot VPD - LE \cdot (\Delta + \gamma)} \tag{5}$$

γ is the psychrometric constant $(\mathrm{kPa\ K^{-1}})$, Δ is the derivative of the saturation pressure curve $(\mathrm{kPa\ K^{-1}})$, ρ is the air density $(\mathrm{kg\ m^{-3}})$, the available energy A $(\mathrm{W\ m^{-2}})$ is defined as $A = Rn - G - S$, where Rn $(\mathrm{W\ m^{-2}})$ is the net radiation, G $(\mathrm{W\ m^{-2}})$ the soil heat flux and S $(\mathrm{W\ m^{-2}})$ is the sum of all storage fluxes, c_p denotes the specific heat of air at constant pressure $(\mathrm{J\ kg^{-1}\ K^{-1}})$ and VPD is the vapor pressure deficit (kPa).

On the basis of the calculation of G_a and G_s the degree of aerodynamic decoupling between the land surface and the atmosphere can be expressed with the decoupling coefficient Ω [−] (Jarvis and McNaughton, 1986).

$$\Omega = \frac{\frac{\Delta}{\gamma} + 1}{\frac{\Delta}{\gamma} + 1 + \frac{G_a}{G_s}} \tag{6}$$

It can take values between 0 and 1. Values close to 0 indicate that the surface is very well coupled to the atmosphere and thus LE mainly depends on VPD and G_s. By contrast, values closer to the limit of 1 mean that Rn is the dominant factor controlling LE.

For better comparability of the sites with respect to soil moisture, the extractable soil water content SWC_{rel} [−] was calculated:

$$SWC_{rel} = \frac{\theta - \theta_{min}}{\theta_{max} - \theta_{min}} \tag{7}$$

where θ ($m^3\ m^{-3}$) is the daily averaged soil water content and θ_{min}, θ_{max} ($m^3\ m^{-3}$) the annual minimum and maximum soil water content. We calculated a Spearman partial correlation between the midday EF and the surface variables – vapor pressure deficit, air temperature, extractable soil water content, and leaf area index – to account for potential non-linear relationships. This approach enables the identification of dominant drivers of altered land–atmosphere interactions on both daily and seasonal scales.

Table 2
Vegetation height (h_{veg}), roughness length (z_0) and receptor height (z_m) used for footprint modeling at each site.

Site	Season	h_{veg} [m]	z_0 [m]	z_m [m]
Near-natural savanna	Dry	2.5	0.19	7.19
	Rainy	4.3	0.34	7.19
Cropland	Dry	0.07	0.0015	3.15
	Rainy	1.0	0.024	3.15
Degraded grassland	Dry	0.01	0.0008	2.65
	Rainy	0.1	0.008	2.65

3.4. Footprint analysis

To assess the effective area of influence of the measured turbulent fluxes a preliminary footprint analysis was conducted for the first time for the three sites. The footprints were calculated with a backwards trajectory Lagrange model according to Kljun et al. (2015). In this model the roughness sublayer height can reach a maximum height of $12.5 \times z_0$, where z_0 is the roughness length [m]. Therefore, we defined z_0 as $z_0 = \frac{h_{veg}}{12.6}$, to include the dynamics of the vegetation height h_{veg} [m] throughout the year. The value 12.6 was selected for the roughness sublayer height to remain slightly below the maximum. Since the footprint was calculated only for two two-week periods, we used the minimum vegetation height for the dry and the maximum for the rainy season. The parameters used for footprint modeling at each site and season are summarized in Table 2.

The measurement height in the model is defined as $z_m = z_r - z_d$, where z_r is the receptor height and z_d the zero plain displacement height, which was derived from the Brutsaert formulation $z_d = 0.67 \times h_{veg}$. Additional input variables were either measured directly, like the wind direction, or derived from the measurements by the TK3 software such as Obukhov length, boundary layer height, friction velocity and the standard deviation of lateral wind velocity fluctuations. The calculation of the footprints was then carried out with the half hourly data in two week intervals.

3.4.1. Flux footprints

Fig. 2 presents the footprints of the turbulent fluxes for each EC station and for two distinct periods. The delineated areas are shown to be representative of the area of interest, extending up to 150 m upwind of the EC station. The results clearly demonstrate a shift in the predominant wind direction, corresponding to the seasonal variations of the West African Monsoon. During the dry period, northeasterly Harmattan winds are predominant, resulting in a northeastern footprint of the turbulent fluxes relative to the EC stations. Conversely, during the rainy period, southwesterly monsoon winds dominate, leading to a southwestern footprint of the turbulent fluxes relative to the EC stations. Moreover, the variability in footprint shape indicates the underlying heterogeneity of the surrounding land surface conditions at the EC sites. The surrounding vegetation (and land use characteristics) are much more homogeneous at the near-nature savanna site resulting in a more uniform footprint. Despite the inherent challenges associated with inhomogeneous land surfaces, the measurements from the cropland and degraded grassland sites, which exhibit a greater degree of surface inhomogeneity compared to the savanna site, still maintain good representativeness. The outcomes of the footprint analysis indicate that relatively reliable footprints can be determined for the three EC stations, meeting typical WAM and land use characteristics in this region. This ensures the reliability of the turbulent flux measurements across the three ecosystems.

4. Results

Fig. 3 illustrates the seasonal cycles of atmospheric variables, radiative forcing, and surface conditions during the study period (2013 to 2015). A typical seasonality for the Sudanian climate is evident in all variables, characterized by alternating dry (yellow background) and wet seasons (blue background), separated by with transitional monsoon periods (white background).

4.1. Annual water balance characteristics

Annual water balance characteristics differed markedly across the three land-use types (Table 3). At the near-natural savanna, ET ranged from 747 to 1017 mm between 2013 and 2015, closely tracking precipitation (876–1047 mm). The $ET/Prec$ ratio increased from 0.85 in 2013 to 1.04 in 2014 before slightly declining to 0.97 in 2015, indicating that nearly all incoming rainfall was returned to the atmosphere, and in some years ET even exceeded precipitation. At the cropland site, ET totals were consistently lower (534–604 mm) than at the savanna, while precipitation inputs were comparable (782–815 mm). Consequently, $ET/Prec$ ratios remained lower (0.68–0.76), reflecting reduced evaporative losses likely related to seasonal vegetation cover and management effects. The degraded grassland exhibited variable dynamics. In 2013 and 2014, ET (644–711 mm) approached or exceeded precipitation (726–638 mm), producing high $ET/Prec$ ratios (0.89–1.11). In contrast, in 2015 ET declined to 576 mm compared to 877 mm of rainfall, lowering the $ET/Prec$ ratio to 0.66. These interannual variations suggest that water balance at the degraded site is highly sensitive to rainfall variability and vegetation dynamics. The cumulative $ET/Prec$ ratios indicate a general underestimation of evapotranspiration across all sites. At the near-natural savanna, however, nearly the entire precipitation input was returned to the atmosphere via evapotranspiration, with a cumulative ratio of 0.96 (96%).

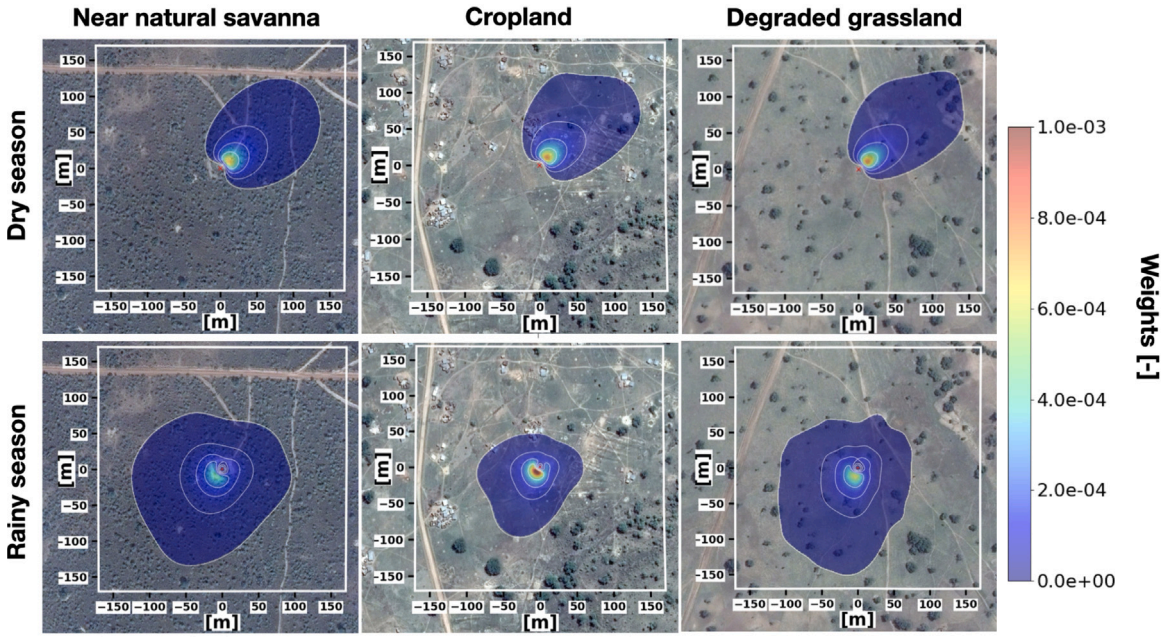

Fig. 2. Flux footprint analysis of EC stations for two representative two-week periods during the dry season (01-01-2015 to 14-01-2015) and the rainy season (15-08-2015 to 29-08-2015), illustrating the origin areas of 80% of the turbulence. The demarcation lines segment the areas into 20% intervals. The colors indicate the weights with which the pixels contribute to the flux of the respective quantity measured at the station. (For interpretation of the references to color in this figure legend, the reader is referred to the web version of this article.)

Table 3
Annual sums of ET, precipitation ($Prec$), and the $ET/Prec$ ratio for the years 2013–2015 at the three sites.

Year	ET [mm]	Prec [mm]	ET/Prec
Near-natural savanna			
2013	747	876	0.85
2014	881	844	1.04
2015	1017	1047	0.97
3-year cumulative ratio:			0.96
Cropland			
2013	560	815	0.69
2014	604	790	0.76
2015	534	782	0.68
3-year cumulative ratio:			0.71
Degraded grassland			
2013	644	726	0.89
2014	711	638	1.11
2015	576	877	0.66
3-year cumulative ratio:			0.86

4.2. Energy balance components and energy partitioning

4.2.1. Multi-year variations and seasonality

Fig. 4 presents the energy balance components for all seasons, averaged over the study period. Significant differences in energy partitioning are evident in the albedo values. A distinct gradient is observed, with the near-natural savanna exhibiting the lowest albedo values across all seasons, followed by cropland, and the degraded grassland showing the highest values. This gradient is most pronounced during the dry-to-wet transitional season with 14% reflection at the near natural savanna, 19% at cropland and 29% at the degraded grassland site (Table 4).

Fig. 5 displays the albedo and the LAI as seven day moving averages. The mentioned gradient of albedo is evident here as well. The differences in albedo between the degraded grassland and the cropland site may be attributed to the higher percentage of bare soil present during the plantation period. Additionally, a clear seasonal pattern of the leaf area index with an inverted gradient compared to the albedo is apparent, ranging from the near-natural savanna, through cropland, to the degraded grassland. As a

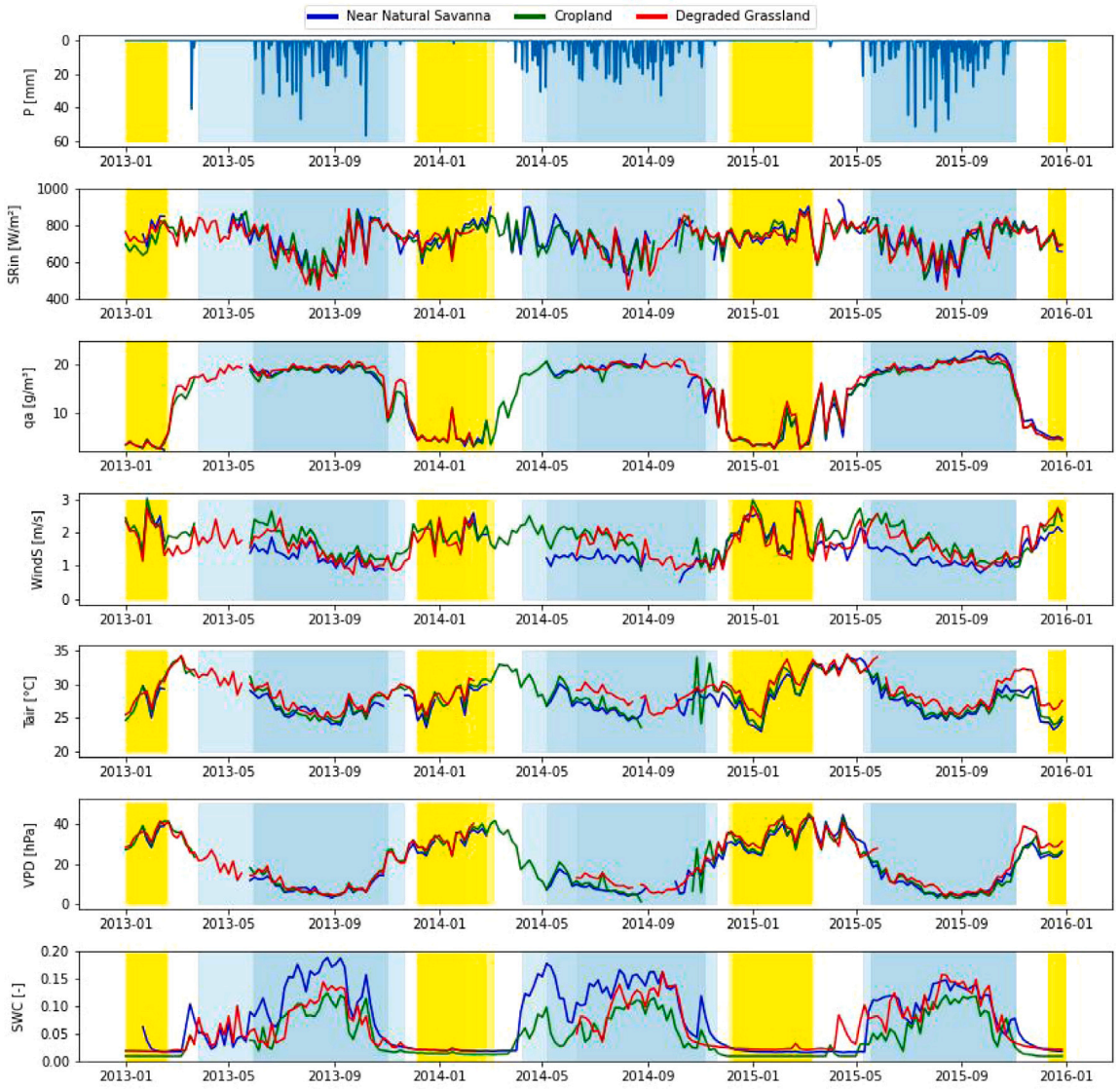

Fig. 3. Daily sums of precipitation (P) and five-day means of incoming shortwave radiation ($SRin$), absolute air humidity (qa), wind speed ($WindS$), air temperature ($Tair$), vapor pressure deficit (VPD) and volumetric soil water content (SWC) for all three stations over the three years period of the study. The yellow and blue background colors indicate the dry and rainy seasons with the transitional periods (white) in between. Note that the start and end dates of these seasons varied slightly between stations. These variations are illustrated by overlaying the delineated periods from all stations with a slight degree of transparency. The most significant discrepancies between the different start and end dates of the seasons, however, arise from data gaps. (For interpretation of the references to color in this figure legend, the reader is referred to the web version of this article.)

consequence of these different reflective properties we can observe a reduction of the Rn on a seasonal scale in Fig. 4,as well as in the continuous time series displayed in Fig. 6.

When examining the turbulent fluxes, the variation among sites becomes less pronounced. H, however, follows the same pattern as the Rn during periods of low vegetation cover, such as the dry season and the subsequent dry-to-wet transitional period (Figs. 4 and 6, Table 4). During the rainy season, H is quite similar across all sites, with slightly higher values at the near-natural savanna, where the highest Rn was recorded. In the wet-to-dry transitional period, the cropland site exhibits the highest H. During this period, groundnuts planted around the cropland site are harvested, leaving the soil bare with no vegetation cover. LE exhibits very similar absolute values at the cropland and degraded grassland sites, but significantly higher values at the near-natural savanna across all seasons (Figs. 4 and 6, Table 4). The partitioning of the absorbable energy into LE and H becomes more apparent when considering EF. EF, as shown in Fig. 6, is significantly higher during both transitional periods and the dry season at the near-natural savanna site compared to the other sites. Cropland and degraded grassland display very similar values across all seasons. During

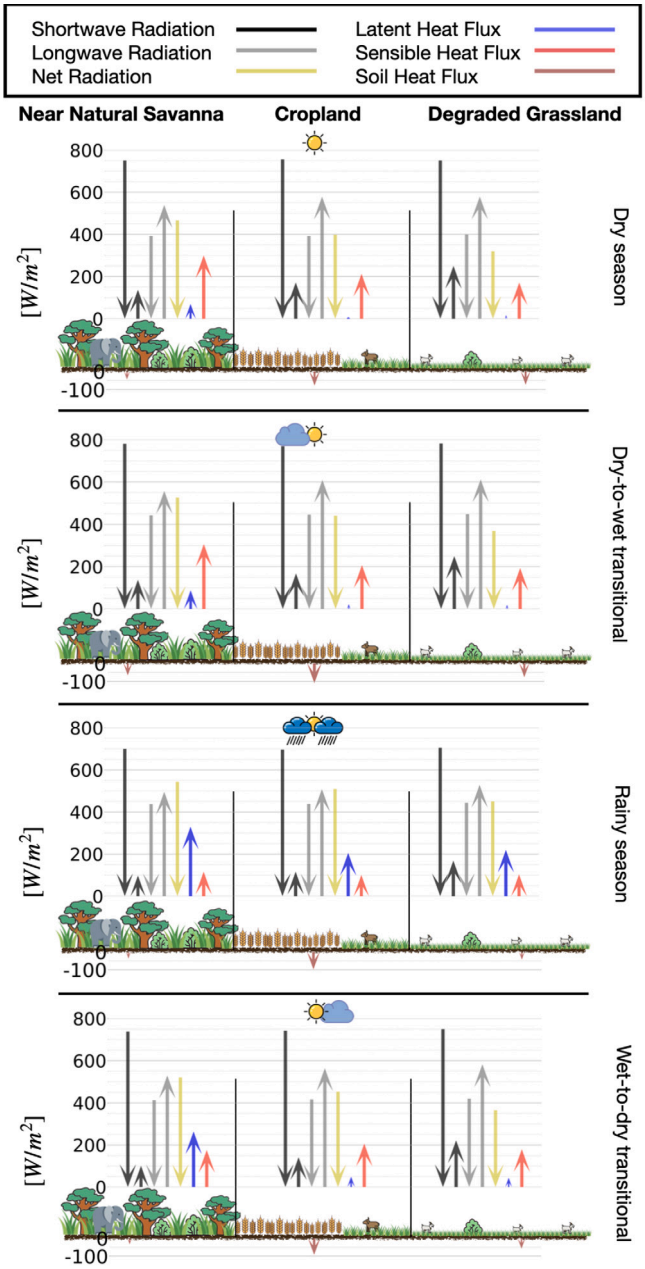

Fig. 4. Seasonal variation of the energy balance components calculated over the three years period from 2013 to 2015. A full monsoonal cycle is displayed from the dry period, the transitional period dry-to-wet, the rainy season to the next transitional period wet-to-dry. The seasonal means are calculated with midday averages.

the dry-to-wet transition, the seasonal mean EF is 0.22 at the near-natural savanna site and 0.1 at both cropland and degraded grassland. The biggest differences are observed for the wet-to-dry transition, with seasonal averages of 0.60 for the near-natural savanna, 0.19 for cropland, and 0.2 for degraded grassland. Minimal differences in EF is observed during the rainy seasons, with seasonal averages of 0.74 at the near-natural savanna, 0.67 at cropland, and 0.68 at degraded grassland. The lowest EF values are noted at the cropland site during the dry season, due to the lack of vegetation cover following the harvest. For a comparison of EF and EBC across sites and seasons, see Fig. B.12.

4.2.2. Diurnal cycles

Fig. 7 shows the seasonal averages of the composite diurnal cycles of LE and H for all three sites. The highest values of LE during daytime are observed at the near-natural savanna site across all seasons, except during the dry-to-wet transition. In this

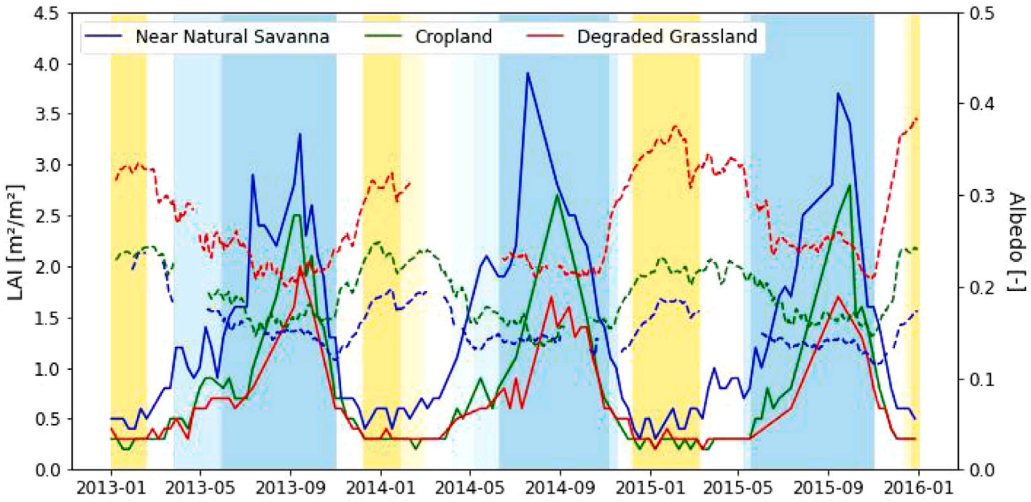

Fig. 5. Seven day moving averages of the leaf area index (solid lines) and the midday means of the albedo (dashed lines) for all three stations. The yellow and blue colors indicate dry and wet seasons and the white parts the respective transitional periods. (For interpretation of the references to color in this figure legend, the reader is referred to the web version of this article.)

Table 4
Seasonal variation of the main energy balance components with means and standard deviation (std) calculated over the three-year period from 2013 to 2015 using midday averages.

	LE [W/m^2]		H [W/m^2]		Rn [W/m^2]		Albedo	
	mean	std	mean	std	mean	std	mean	std
Cropland Dry	14.4	8.3	213.3	30.4	398.2	42.3	0.2	0.01
Degraded Grassland Dry	17.6	16.3	172.1	26.3	320.0	38.4	0.3	0.02
Near Natural Savanna Dry	70.2	37.1	300.3	44.9	466.4	58.4	0.2	0.02
Cropland DryToWet	23.0	52.2	207.2	48.0	440.4	80.1	0.2	0.02
Degraded Grassland DryToWet	19.9	43.5	193.7	38.1	368.4	53.1	0.3	0.02
Near Natural Savanna DryToWet	88.5	42.8	306.9	47.2	526.4	107.7	0.2	0.02
Cropland Rainy	205.7	75.6	101.0	48.4	509.2	133.3	0.2	0.02
Degraded Grassland Rainy	220.3	103.0	103.9	55.4	450.3	117.4	0.2	0.03
Near Natural Savanna Rainy	330.1	92.6	116.5	48.1	543.5	138.8	0.1	0.07
Cropland WetToDry	49.8	31.5	206.6	31.9	452.6	68.9	0.2	0.02
Degraded Grassland WetToDry	44.5	27.18	179.9	18.2	364.9	59.3	0.3	0.04
Near Natural Savanna WetToDry	264.3	100.63	175.9	50.5	519.8	63.0	0.1	0.01

period, the LE at the savanna site increases sharply shortly after sunrise, then levels off, converging with the maximum observed at the degraded grassland site by noon. The degraded grassland site exhibits higher midday maxima of LE than the cropland site during both the dry-to-wet transition and the rainy season. This difference can be explained by the land management at the cropland site, leaving the soil bare after harvest and tillage at the end of the rainy season. These fluxes also persist longer into the evening hours at the degraded grassland site.

H shows its most negative values at the near-natural savanna at night, particularly during the dry season, indicating more efficient surface cooling through higher daytime LE compared to the altered sites. This effect is also seen in the faster evening decrease of H at the near-natural savanna site as radiative forcing decreases. During the wet-to-dry transitional period, characterized through a dense vegetation cover and a high LE, this leads to a brief minimum in H shortly after sunset, rebounding within an hour once the heat gradient between the surface and atmosphere is reduced.

4.3. Drivers of altered land–atmosphere interactions

The relationship between EF and VPD is most pronounced during the transitional periods at the altered land use sites cropland and degraded grassland (Fig. 8). It is during these periods that the slopes of the regression line indicate a high sensitivity of EF to changes in VPD. This increased sensitivity is attributed to stronger surface–atmosphere coupling at these sites compared to the near natural savanna site, as will be demonstrated in the next chapter. The confidence intervals reveal a pronounced scattering of values at the altered sites, with the strongest scattering of values observed at the degraded grassland site. During the dry season, when the VPD reaches its maximum value, EF at the near natural savanna site remains relatively high. This could be explained by

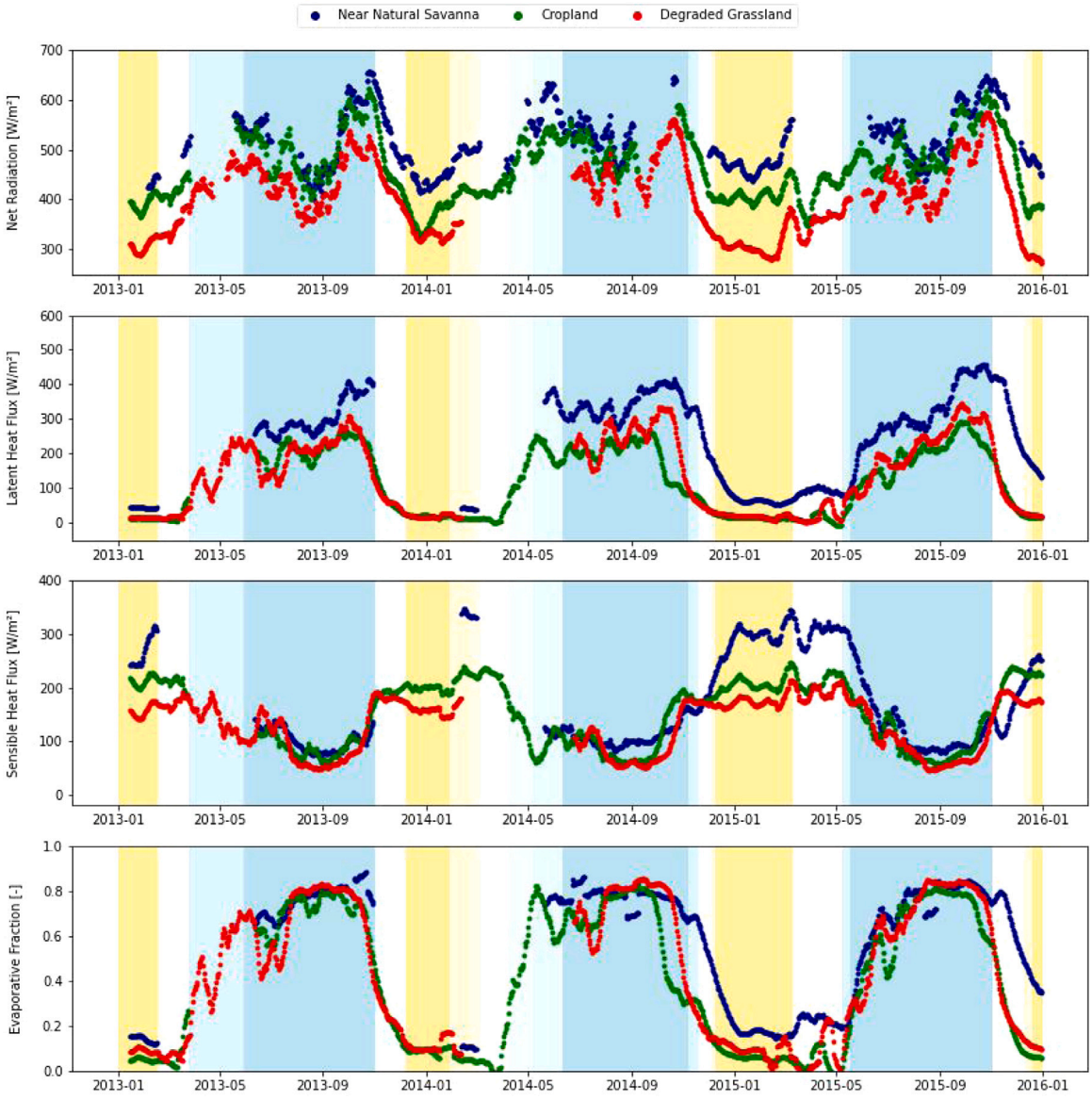

Fig. 6. 15-days moving averages of Rn, LE and H and EF for all three stations. Averages were calculated over full 24-hour periods.

the presence of evergreen vegetation, which potentially maintains LE through root water uptake from deeper soil layers. However, partial correlation analysis reveals that VPD is significantly associated with EF only at the degraded grassland site, albeit with a low correlation coefficient of 0.12, as summarized in Fig. 9. This suggests that while VPD is related to EF in this setting, its independent contribution remains limited, likely due to its strong dependence on air temperature.

The relationship between EF and LAI shows a positive correlation at all sites. The slope of the regression line is considerably steeper at the altered sites, indicating a strong dependence of LE on vegetation cover dynamics. The highest partial correlation is observed at the degraded grassland site (r = 0.54), followed by the near-natural savanna site (r =0.39). In contrast, the cropland site shows a comparatively weak partial correlation (r = 0.21), as illustrated in Fig. 9.

With respect to SWC_{rel} all sites exhibit a critical threshold above which EF becomes largely independent of soil moisture. Below this threshold, a strong dependence of SWC_{rel} to EF can be observed, particularly for the agricultural site. This is reflected in the partial correlation coefficients of $r = 0.53$ for cropland and $r = 0.58$ for degraded grassland. At lower soil moisture levels, all sites show high variability, especially during the transitional periods, likely due to water uptake and transpiration dynamics of the present vegetation.

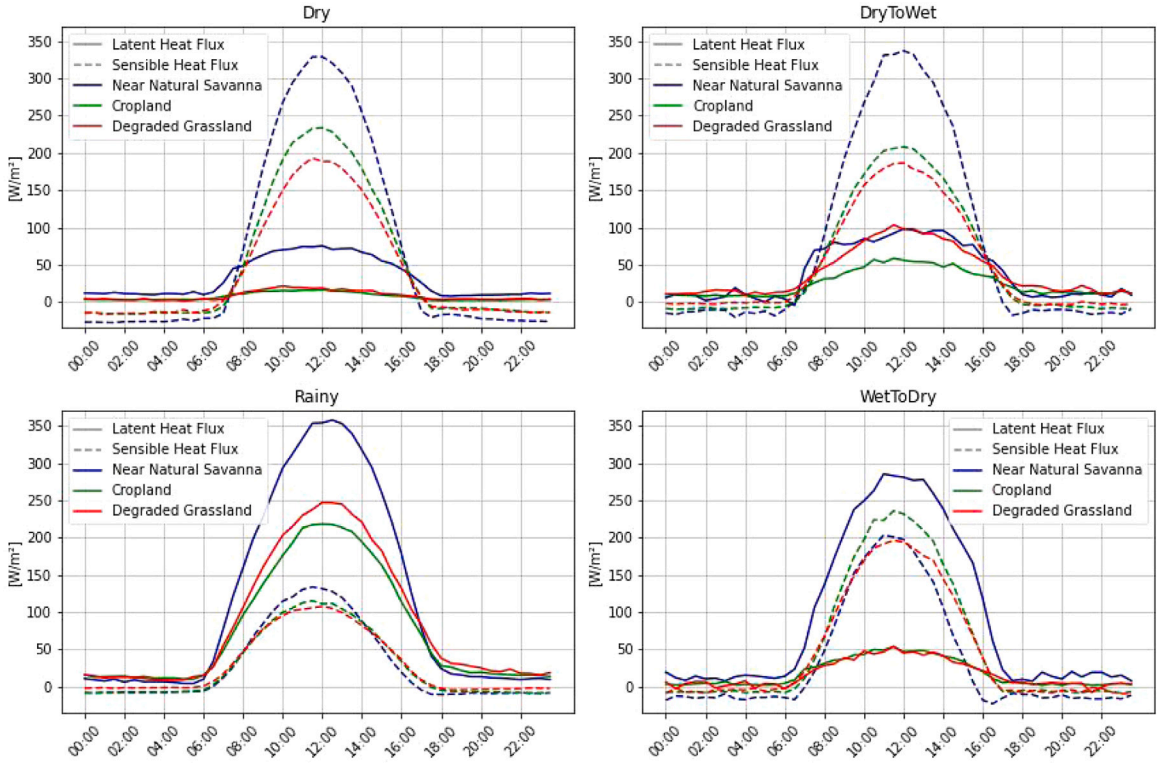

Fig. 7. Composite diurnal cycles of turbulent fluxes at the three study sites during different seasons, averaged over the period 2013–2015. Solid lines represent LE, while dashed lines represent H.

4.4. Land–atmosphere coupling properties

In Fig. 10 the surface conductance (G_s), the aerodynamic conductance (G_a) and the decoupling coefficient (Ω) calculated with midday means are displayed. The surface conductance shows a clear seasonal cycle at all three land use types, with the highest variability and maxima during the rainy season, reaching up to 35 mm/s. During the dry season, the surface conductance remains stable at very low values, close to zero, at the altered land use sites. The near-natural savanna site consistently shows the highest values across all season, while the other two sites differ only slightly. Those differences to the altered sites are most apparent during the rainy season and the subsequent drying season, as shown in Fig. 11, where seasonal means are displayed. During the beginning of the rainy season, G_s increases faster at the near-natural savanna compared to the altered sites and decreases slower during the wet-to-dry transitional period.

The seasonality of the aerodynamic conductivity (G_a) differs significantly from G_s and between the sites. G_a shows less pronounced seasonal cycles, and its values are more stable across the different seasons and land use types. In Fig. 11 we observe clear maxima during both transitional periods at the near-natural savanna with around 120 mm/s. The lowest values, around 100 mm/s, occurred during the dry period, which is similar to the rainy season.

The decoupling coefficient Ω shows a similar seasonal cycle to surface conductance, with minima around 0.03 during the dry and dry-to-wet transitional seasons, indicating that the surface is fully coupled to the atmosphere at all sites. Here, LE is governed purely by vapor pressure deficit and Rn. During the rainy season, the seasonal mean Ω reaches about 0.35 (Fig. 11), with daily values occasionally approaching 1 (Fig. 10), indicating a high degree of surface decoupling from the atmosphere. In this case, LE is primarily controlled by vegetation physiology. During the wet-to-dry transitional period, the decoupling at the near-natural savanna site decreases more slowly than at the other sites due to its dense vegetation cover, as reflected in the dynamics of the LAI (Fig. 5).

5. Discussion

Overall, the three sites illustrate distinct hydrological behavior: while the near-natural savanna sustained a high and stable evaporative demand, cropland consistently exhibited reduced evapotranspiration relative to rainfall, and the degraded grassland alternated between excessive evaporative losses and rainfall surplus, highlighting its instability in water balance functioning. Across sites, EF was primarily driven by soil moisture and LAI. While the role of surface soil moisture is comparatively well understood and widely represented in ecohydrological models, vegetation phenology and leaf area dynamics introduce greater complexity. Correlations indicate that grasslands show a stronger link between LAI and EF than savannas, where variability in tree cover

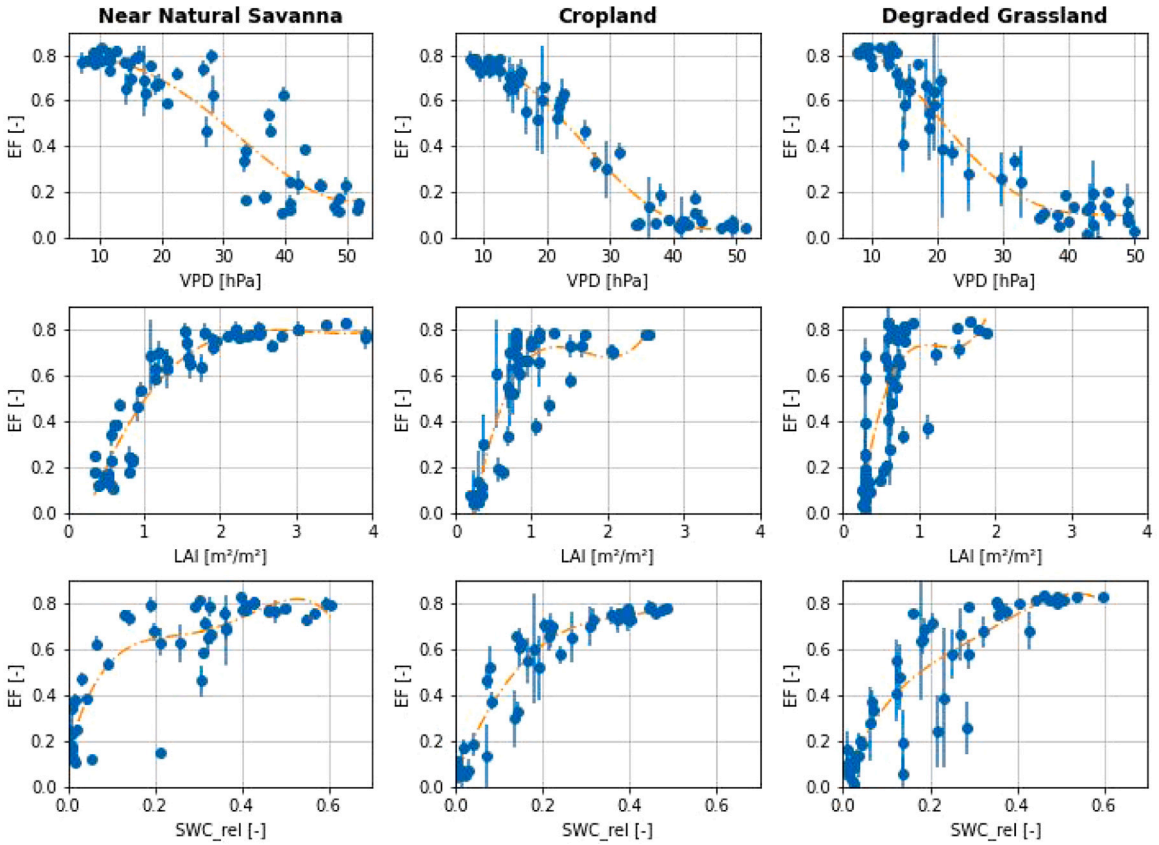

Fig. 8. 14-days bins and 95% confidence interval (vertical bars) showing the dependency of EF with VPD, LAI and SWC_{rel} for the three EC sites.

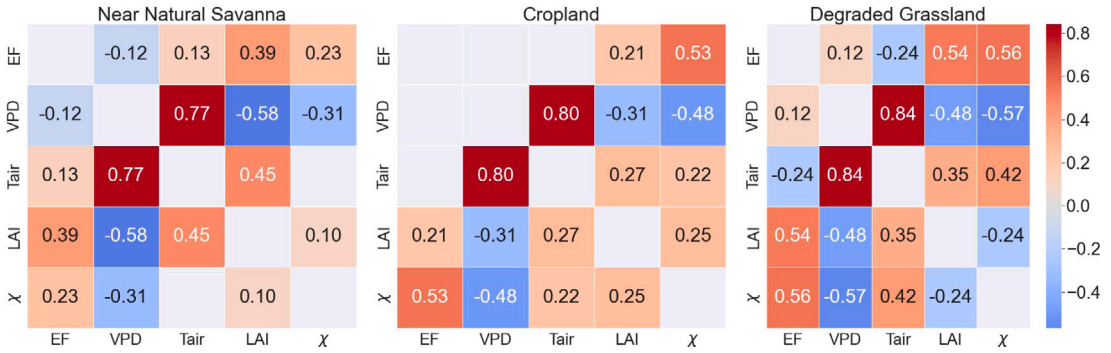

Fig. 9. Spearman partial correlations calculated over the three-year period showing significant relations between EF and some physical predictor variables (VPD = vapor pressure deficit; $Tair$ = air temperature; LAI = leaf area index; $\boldsymbol{SWC_{rel}}$ = extractable soil water content). Only coefficients for $p < 0.01$ are displayed.

adds additional layers of complexity. Recent advances, such as phenocam monitoring of local tree and grass phenology, provide promising avenues for improving our understanding of these vegetation–atmosphere interactions.

5.1. Vegetation structure and albedo dynamics

The analysis of the energy balance components reveals a substantial increase in albedo at the degraded grassland site, driven by variations in vegetation characteristics across the three locations. These differences in vegetation are also reflected in the remotely-sensed LAI data from the EC sites. The high albedo values observed at the degraded grassland site particularly during the dry season

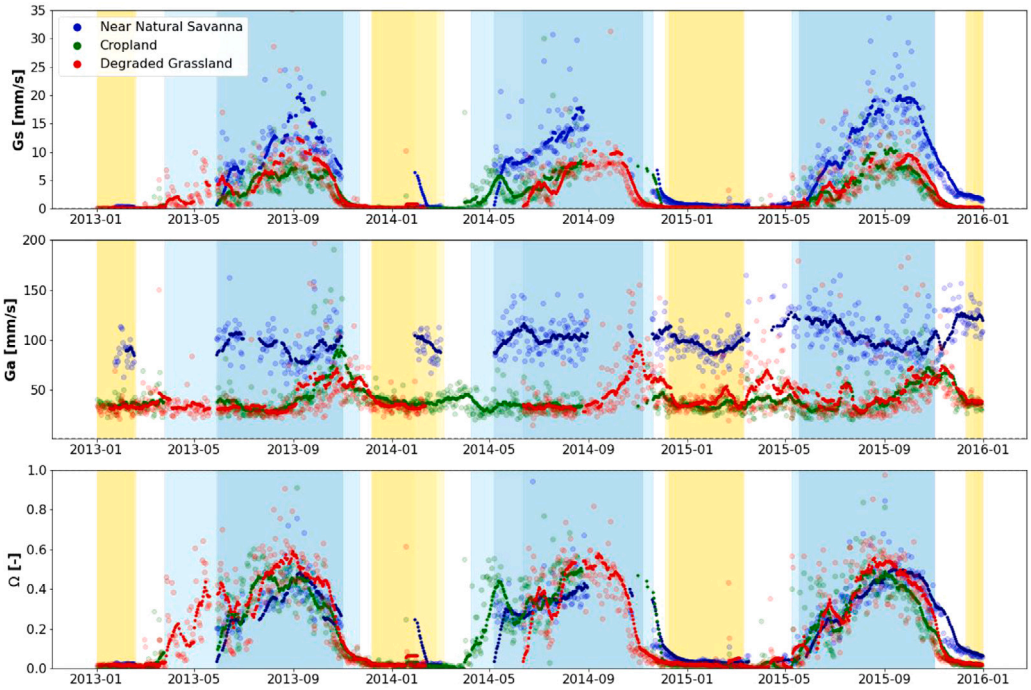

Fig. 10. Midday (10:00 to 14:00) daily means (transparent dots) and midday 15-days moving averages (solid dots) of surface conductance, aerodynamic conductance and the decoupling coefficient.

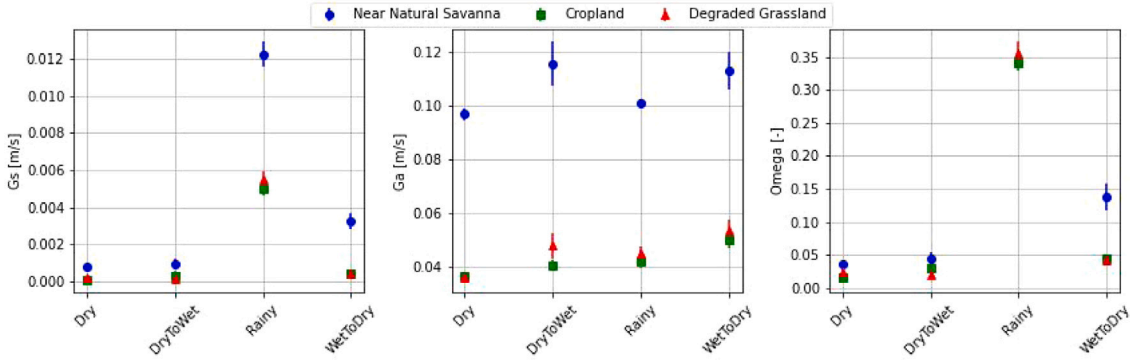

Fig. 11. Seasonal means of surface conductance, aerodynamic conductance and decoupling coefficient averaged over the three years study period for all three stations. The error bars represent the 95% confidence interval.

can be attributed to the high grazing pressure and the subsequent little amount of phytomass covering the relatively bright soils according to Samain et al. (2008). Grazing likely also contributes to the irregular peaks of LAI at this site, reflecting inconsistent vegetation growth and limited recovery capacity. With the increase in LAI during the transition from the dry to the wet season, albedo decreases at all sites due to plant growth and the reduction of surface albedo by wet soils (Samain et al., 2008). As a result, the smallest differences in albedo are observed during the rainy season, when it reaches its minimum across all study sites. The pronounced albedo gradient leads to a corresponding gradient in Rn. These results are consistent with the studies by Timouk et al. (2009) and Mamadou et al. (2016). Together, the albedo and LAI patterns highlight the fundamental role of vegetation structure and management in shaping site-specific surface energy exchange, and help explain the differing strengths of the EF–LAI relationships across ecosystems.

5.2. Energy balance components across land use types

The differences of the energy balance components between the degraded grassland and cropland site are less pronounced. Although Rn is consistently and significantly higher at the cropland site compared to the degraded grassland site. However, this

difference is only slightly reflected in the absolute values of the turbulent fluxes. The cropland site shows only marginally higher H values during the dry season and both transitional seasons. Part of the Rn at the cropland site contributes to soil heat flux, which exhibits the highest values at this site during all seasons. In contrast to Ceperley et al. (2017), who found higher H over a savanna forest year-round in Burkina Faso, we observed increased H over the near-natural savanna only during the dry and dry-to-wet transitional seasons. This difference is likely due to local factors such as the presence of bare rocks in their study area, which enhance H development but are absent at our near-natural site. We find good agreement in H with Brümmer et al. (2008b), whose study site in southeastern Burkina Faso is comparable to our near-natural site, as well as with the agricultural and open woodland sites studied in Mamadou et al. (2016).

5.3. Diurnal patterns and transpiration responses

Distinct patterns were observed in the diurnal dynamics of the LE. During the dry-to-wet transitional season, the near natural savanna exhibited a sharp increase in LE after sunrise, which then leveled off, ultimately reaching similar maximum values as observed at the degraded grassland. Brümmer et al. (2008a) and Linstädter (2009) showed that this pattern is due to the rapid response of the relatively dense vegetation (LAI between 0.5 and 1 compared to 0.3 to 0.4 at the two altered sites, see Fig. 5) to the early morning solar radiation, which quickly boosts transpiration. Later in the day the vegetation closes its stomata to safe water leading to a limited LE, which therefore does not follow the bell shaped curve of the energy input. Between the agricultural sites, we observed a higher midday maximum of the LE at the degraded grassland site compared to cropland. The vegetation of the degraded grassland site can recover faster with the first rain events leading to higher transpiration rates (Liu et al., 2008; Baldocchi et al., 2004). Additionally, grass generally exhibits the highest transpiration rates among the different species of savanna vegetation, as demonstrated with growth chamber experiments by Belovitch et al. (2023).

5.4. Energy partitioning and evapotranspiration efficiency

The EF analysis revealed that energy partitioning was relatively similar at both altered sites. However, significant differences were observed when compared to the near-natural savanna site during both transitional seasons and the dry season. During the dry season, the EF at the savanna site, averaged over a three-year period, was 2.9 times higher than at the cropland site and 2 times higher than at the degraded grassland site. During the dry-to-wet transition, these factors were 2.6 for cropland and 2.9 for degraded grassland. For the wet-to-dry transition, the factor was 3.14 for both sites. These values are similar with those reported in previous studies like Guyot et al. (2012), Mamadou et al. (2016) and Ceperley et al. (2017). The strong dependence of EF on vegetation dynamics aligns with findings from other water-limited regions, where shallow-rooted grasses exhibit rapid transpiration responses to rainfall, whereas deeper-rooted systems can buffer moisture stress and sustain evapotranspiration during dry periods (Hanan and Lehmann, 2010).

At the near-natural savanna, energy partitioning favored LE more prominently, attributed to denser vegetation and a higher presence of trees and bushes. These plants can access water from deeper soil layers for evaporation, enhancing LE. These findings align with Restrepo-Coupe et al. (2013), who demonstrated, that areas converted from forest to cropland and pasture exhibit different behaviors, including relative reductions in dry season evapotranspiration due to increased water limitations from the loss of deep roots accessing soil water. The analysis further reveals that the energy partitioning represented by EF, exhibit the strongest dependence on the dynamics of the vegetation cover at the degraded grassland site, followed closely by the near natural savanna site. The weakest dependence was observed at the cropland site, where bare soil evaporation after tillage likely accounts for a substantial portion of LE. Those bare soil periods may not be accurately captured in the satellite derived LAI, due to its relatively low resolution compared to the area of influence of the flux measurements. Additionally, the water content of the upper soil layer significantly influenced EF at both altered sites, whereas this influence was considerably lower at the near-natural savanna, once again highlighting the influence of trees and bushes with deep roots on the energy partitioning. The observed high correlation at the degraded grassland site can be explained with the previously mentioned elevated transpiration rate of savanna grass species (Belovitch et al., 2023). Moreover the determined correlations align with those reported in Mamadou et al. (2016).

5.5. Vegetation control and coupling in land–atmosphere exchange

The analysis of land–atmosphere exchange coefficients showed similar results as those reported in Mamadou et al. (2014), but considerably lower values as in Bagayoko et al. (2007). A sharp increase of the surface conductance at the beginning of the rainy season at all sites is caused by the rapid increase in green vegetation, mainly savanna grass, with the arrival of the first rains. Spank et al. (2016) found, however, that the relative curves of surface conductance and canopy height align only at the beginning of the growing season. During the subsequent phenological development stages, even before the ripening stage, significant divergences occur between the two curves.

The analysis of the decoupling coefficient Ω showed that highest values are reached during the rainy season, indicating, that the physiology of the vegetation cover is predominantly governing LE (Spank et al., 2016). A pronounced difference to Mamadou et al. (2014) was only found for the aerodynamic conductivity at the cultivated sites. Our cultivated site shows lower values, likely due to variations in land management practices, vegetation cover and climatic conditions. Towards the end of the rainy season, there is a notable spike in aerodynamic conductivity at both altered sites. This occurs when Rn reaches peak values (Fig. 6), leading to increased air temperature and vapor pressure deficit values (Fig. 3). These conditions create more unstable atmospheric situations, enhancing turbulence therefore increasing aerodynamic conductivity. This spike may reflect intensified land–atmosphere interactions, potentially driven by heightened thermal and moisture gradients during this period.

5.6. Study limitations

While the present study focuses on differences in land–atmosphere exchange among sites, we acknowledge that the energy balance closure introduces uncertainty into the interpretation of absolute flux magnitudes. Previous work on the same sites by Nadolski et al. (2024) demonstrated systematic underestimations of 10%–30% in the turbulent energy fluxes, with the best closure observed at the near-natural savanna and the poorest at the cropland site. These differences in EBC are partly attributed to land use heterogeneity and surface conditions. Importantly, seasonal patterns and relative differences in flux partitioning between sites were consistent despite the varying closure rates. Therefore, although limitations in energy balance closure may affect the precision of absolute flux estimates, we consider the identified patterns, particularly the comparative behavior of the ecosystems and the influence of vegetation structure on energy partitioning, as meaningful. Nonetheless, their robustness should be further evaluated in future studies.

While we acknowledge the limitations of MODIS LAI in heterogeneous savanna landscapes due to its coarse spatial resolution (500 m) and potential mismatch with local station footprints, it nonetheless captures distinct differences between the sites in our study. We interpret this not as a precise, local measurement of canopy structure, but as a useful indicator of broader vegetation patterns across ecosystems. Similar conclusions were drawn by Mayr and Samimi (2015), who found that although MODIS LAI tends to overestimate absolute values and is insensitive to small-scale disturbances (e.g. fire), it still reliably represents regional spatial patterns when compared with field measurements and high-resolution LAI models.

Caution is warranted when interpreting ET patterns, as uncertainties stem both from gap-filling procedures using land surface model simulations and from the interpolation of precipitation data used as input for the model. These processes may introduce biases that influence the absolute magnitude of fluxes and water balance estimates, thereby contributing to uncertainties in the calculated annual hydrological budgets. Similar care is required when interpreting soil heat flux data, since the representativeness of the measurement location is limited at the altered sites. Vegetation above the heat flux plates within the fenced EC areas could not always be maintained consistently with the surrounding fields (Bliefernicht et al., 2018). For example, during groundnut cultivation at the cropland site, fallow vegetation was present inside the fenced area.

5.7. Implications for boundary layer processes and climate modeling

Notably, the flux of water from the surface to the atmosphere was shown to decrease substantially when vegetation shifts from near-natural savanna to a more degraded state, resulting in a drier and more stable boundary layer (Stull, 2012). These changes in boundary layer stability may influence cloud formation and related processes such as precipitation (Jung and Kunstmann, 2007; Heinzeller et al., 2018; Sun et al., 2023). In turn, such alterations can affect other critical land surface processes, including groundwater recharge and evaporative cooling. The complexity of these interactions, along with the critical role of land use and vegetation structure, highlights the need for further detailed investigations using this unique EC experiment in this understudied region. Accurately representing these processes and their small-scale variability in climate models can lead to more precise predictions and enhance the overall predictability of the West African climate (Xue et al., 2012).

6. Summary and conclusion

In this study the impact of land use change was analyzed for three contrasting savanna sites in West Africa using a unique micro-meteorological experiment based on eddy covariance towers. We demonstrate that land use and vegetation structure is of central importance for the characteristics of the energy and water fluxes on the land surface and for land–atmosphere interactions. Changes in land surface characteristics can significantly impact the exchange of water, heat, and momentum between the land and the atmosphere, as illustrated by this EC experiment. The key findings of this study are as follows:

1. Significant disparities were observed in radiation variables such as albedo (up to 30%) and Rn (up to 45%), and turbulent fluxes across contrasting land use sites, particularly on seasonal and diurnal scales. Notably, during the dry season and both transitional phases of the West African Monsoon, the energy partitioning in terms of EF is markedly altered (up to 30%), exhibiting much lower heat fluxes at agricultural sites compared to the near natural savanna.
2. Smaller differences in EF were observed between degraded grassland and cropland, primarily due to the distinct physiological properties of the vegetation and differences in land management practices. The degraded grassland site is used exclusively for grazing, resulting in a consistently low grass layer throughout the year. In contrast, crop cycles at the cropland site lead to periods of bare soil after tillage and greater variability in vegetation height compared to the grassland site.
3. Our exploration into the potential drivers of land–atmosphere interactions, using partial correlation analysis, indicate clear differences between the sites: (a) The degraded grassland site exhibited the highest sensitivity of the EF to LAI indicated by a stronger correlation (r = 0.54) likely due to the high abundance of savanna grass. (b) Soil moisture in the upper layers exerts a significant control on evapotranspiration at both altered sites, as indicated by partial correlation coefficients of $r = 0.53$ and $r = 0.56$. In contrast, the savanna site showed much lower correlations (r = 0.23), most likely pointing towards the relevant contribution of water uptake through deep roots.
4. The study revealed that land–atmosphere coupling is primarily altered during the drying phase of the WAM.
5. Furthermore, our analysis showed that the physiological differences, as described by surface conductance, were significant between the near-natural savanna and the altered sites during the rainy season and the wet-to-dry transitional period, with values around three times higher at the near-natural savanna compared to the altered sites.

Table A.5
Number of H and LE measurements before and after filtering of values flagged with low reliability by the TK3 software over the three-year study period (2013–2015) at the three study sites.

	H		LE	
	Before filtering	After filtering	Before filtering	After filtering
Near Natural Savanna	29,235	27,424	27,883	27,379
Cropland	39,614	36,572	37,159	36,560
Degraded Grassland	33,586	31,377	32,095	31,345

6. The aerodynamic properties were distinct between the savanna site and the altered sites throughout the year, with seasonal mean values of aerodynamic conductance ranging from 95 to 120 mm/s at the near-natural savanna and from 30 to 50 mm/s at the altered sites. The differences between the altered sites were minimal.
7. The calculated footprints, encompassing the areas from which 80% of the fluxes measured at the station originate, extend up to 150 m upwind. They reveal consistent seasonal patterns and highlight notable differences between sites with varied land uses, thereby confirming the representativeness of our data for the targeted areas.

Overall, our study bridges critical knowledge gaps by providing ground-based evidence on how land use influences land–atmosphere interactions in the West African Sudanian savanna. These insights are not only essential for refining regional climate and hydrological models but also carry practical significance for climate adaptation, sustainable land management, and water resource planning in a region facing rapid environmental change.

CRediT authorship contribution statement

Luitpold Hingerl: Writing – original draft, Visualization, Methodology, Investigation, Formal analysis, Data curation, Conceptualization. **Jan Bliefernicht:** Writing – review & editing, Writing – original draft, Project administration, Methodology, Conceptualization. **Samuel Guug:** Writing – review & editing, Data curation. **Souleymane Sy:** Writing – review & editing. **Frank Neidl:** Data curation. **Thomas Jagdhuber:** Writing – review & editing. **Harald Kunstmann:** Writing – review & editing, Supervision, Conceptualization.

Acknowledgments

The author(s) declare that financial support was received for the research, authorship, and/or publication of this article. This work was part of the WASCAL (West African Science Service Center on Climate Change and Adapted Land Use, www.wascal.org), granted by the Federal Ministry of Education and Research in Germany (grant number: 01LG1202C1). This research is also supported by the Federal Ministry of Education and Research of Germany (BMBF) through the Concerted Regional Modeling and Observation Assessment for Greenhouse Gas Emissions and Mitigation Options under Climate and Land Use Change in West Africa (CONCERT-West Africa; grant number 01LG2089A BMBF). Special thanks goes to Björn Lund who performed the Noah LSM simulations and closed the data gaps of the meteorological time series. We further thank Matthias Mauder for the support in the eddy covariance technique and the introduction to the TK3 software.

Declaration of competing interest

The authors declare that they have no known competing financial interests or personal relationships that could have appeared to influence the work reported in this paper.

Appendix A. Measurement counts before and after quality filtering.

See Table A.5

Appendix B. Assessing the reliability of evaporative fraction across land use types

See Fig. B.12.

Data availability

Data will be made available on request.

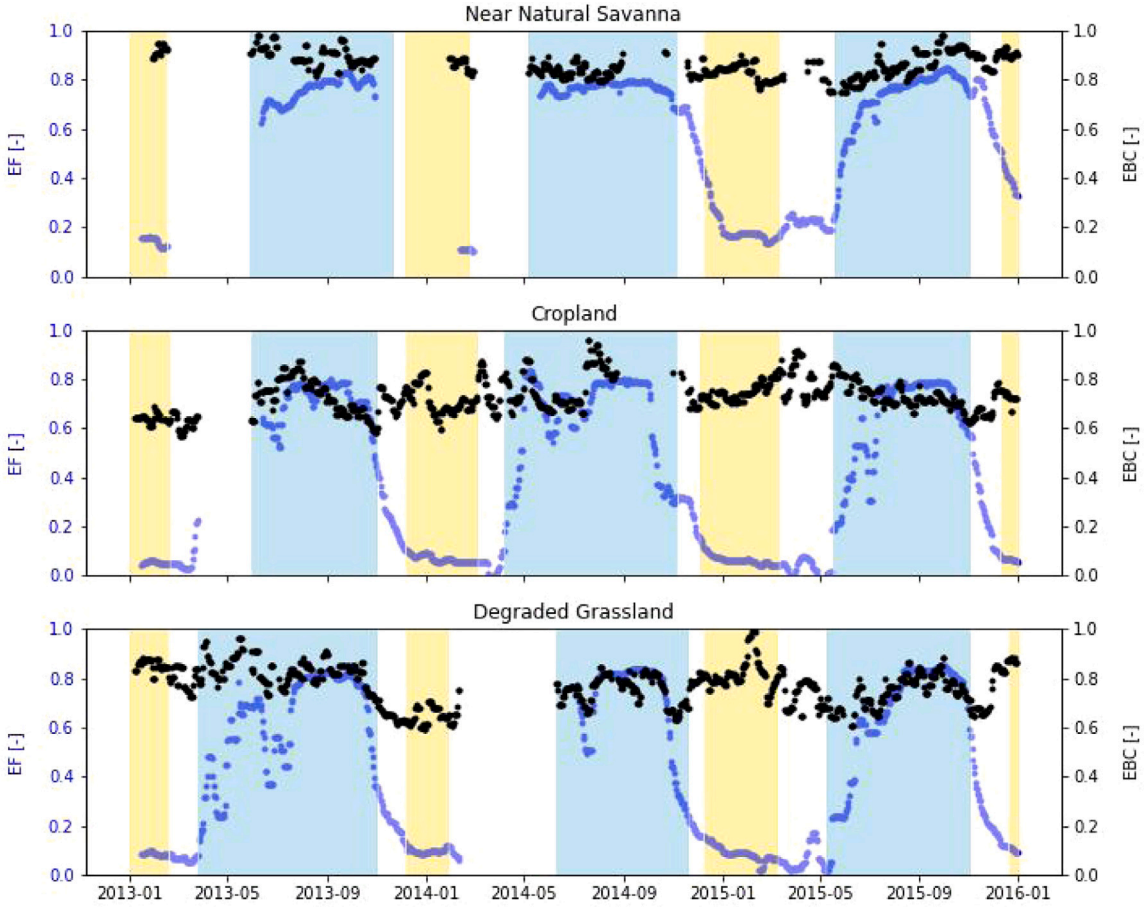

Fig. B.12. Temporal evolution of EF and EBC across three land use types. Rolling medians (7-day) highlight site-specific EF patterns that remain consistent across seasons and years, despite differences in EBC. While EBC is highest at the near-natural savanna and lower at the cropland and degraded grassland, EF consistently reflects vegetation-driven energy partitioning. This suggests that EF can serve as a robust comparative indicator, though interpretation should account for uncertainties related to incomplete energy balance closure and site-specific measurement challenges.

References

Allies, A., Olioso, A., Cappelaere, B., Boulet, G., Etchanchu, J., Barral, H., Moussa, I.B., Chazarin, J.P., Delogu, E., Issoufou, H.B.A., 2022. A remote sensing data fusion method for continuous daily evapotranspiration mapping at kilometric scale in Sahelian areas. J. Hydrol. 607, 127504.

Arnault, J., Mwanthi, A.M., Portele, T., Li, L., Rummler, T., Fersch, B., Hassan, M.A., Bahaga, T.K., Zhang, Z., Mortey, E.M., 2023. Regional water cycle sensitivity to afforestation: synthetic numerical experiments for tropical Africa. Front. Clim. 5, 1233536.

Bagayoko, F., Yonkeu, S., Elbers, J., van de Giesen, N., 2007. Energy partitioning over the west african savanna: Multi-year evaporation and surface conductance measurements in Eastern Burkina Faso. J. Hydrol. 334 (3–4), 545–559.

Baldocchi, D.D., Xu, L., Kiang, N., 2004. How plant functional-type, weather, seasonal drought, and soil physical properties alter water and energy fluxes of an oak-grass savanna and an annual grassland. Agric. For. Meteorol. 123 (1–2), 13–39.

Belovitch, M.W., NeSmith, J.E., Nippert, J.B., Holdo, R.M., 2023. African savanna grasses outperform trees across the full spectrum of soil moisture availability. New Phytol. 239 (1), 66–74.

Berger, S., Bliefernicht, J., Linstädter, A., Čanak, K., Guug, S., Heinzeller, D., Hingerl, L., Mauder, M., Neidl, F., Quansah, E., Salack, S., Steinbrecher, R., Kunstmann, H., 2019. The impact of rain events on CO2 emissions from contrasting land use systems in semi-arid West African savannas. Sci. Total. Environ. 647, 1478–1489. http://dx.doi.org/10.1016/j.scitotenv.2018.07.397.

Bliefernicht, J., Berger, S., Salack, S., Guug, S., Hingerl, L., Heinzeller, D., Mauder, M., Steinbrecher, R., Steup, G., Bossa, A.Y., 2018. The WASCAL hydrometeorological observatory in the Sudan Savanna of Burkina Faso and Ghana. Vadose Zone J. 17 (1), 1–20.

Bliefernicht, J., Kunstmann, H., Hingerl, L., Rummler, T., Andresen, S., Mauder, M., Steinbrecher, R., Friess, R., Gochis, D., Gessner, U., 2013. Field-and Simulation Experiments for the Investigating regional Land-Atmosphere Interactions within the West Africa: experimental set-up and first results. IAHS Publ. 359 (2013), 226–232.

Bliefernicht, J., Salack, S., Waongo, M., Annor, T., Laux, P., Kunstmann, H., 2022. Towards a historical precipitation database for West Africa: Overview, quality control and harmonization.

Blonquist Jr., J., Tanner, B., Bugbee, B., 2009. Evaluation of measurement accuracy and comparison of two new and three traditional net radiometers. Agricult. Forest. Meterol. 149 (10), 1709–1721.

Boone, A.A., Xue, Y., Sales, F.D., Comer, R.E., Hagos, S., Mahanama, S., Schiro, K., Song, G., Wang, G., Li, S., 2016. The regional impact of Land-Use Land-cover Change (LULCC) over West Africa from an ensemble of global climate models under the auspices of the WAMME2 project. Clim. Dyn. 47, 3547–3573.

Brümmer, C., Brüggemann, N., Butterbach-Bahl, K., Falk, U., Szarzynski, J., Vielhauer, K., Wassmann, R., Papen, H., 2008a. Soil-atmosphere exchange of N 2 O and NO in near-natural savanna and agricultural land in Burkina Faso (W. Africa). Ecosyst. 11, 582–600.

Brümmer, C., Falk, U., Papen, H., Szarzynski, J., Wassmann, R., Brüggemann, N., 2008b. Diurnal, seasonal, and interannual variation in carbon dioxide and energy exchange in shrub savanna in Burkina Faso (West Africa). J. Geophys. Res.: Biogeosciences 113 (G2).

Ceperley, N.C., Mande, T., Van De Giesen, N., Tyler, S., Yacouba, H., Parlange, M.B., 2017. Evaporation from cultivated and semi-wild Sudanian Savanna in west Africa. Hydrol. Earth Syst. Sci. 21 (8), 4149–4167.

Duveiller, G., Caporaso, L., Abad-Viñas, R., Perugini, L., Grassi, G., Arneth, A., Cescatti, A., 2020. Local biophysical effects of land use and land cover change: towards an assessment tool for policy makers. Land Use Policy 91, 104382.

Ek, M., Mitchell, K., Lin, Y., Rogers, E., Grunmann, P., Koren, V., Gayno, G., Tarpley, J., 2003. Implementation of Noah land surface model advances in the national centers for environmental prediction operational mesoscale Eta model. J. Geophys. Res.: Atmospheres 108 (D22).

Flörke, M., Schneider, C., McDonald, R.I., 2018. Water competition between cities and agriculture driven by climate change and urban growth. Nat. Sustain. 1 (1), 51–58.

Fratini, G., Mauder, M., 2014. Towards a consistent eddy-covariance processing: an intercomparison of EddyPro and TK3. Atmospheric Meas. Tech. 7 (7), 2273–2281.

Galle, S., Grippa, M., Peugeot, C., Moussa, I.B., Cappelaere, B., Demarty, J., Mougin, E., Panthou, G., Adjomayi, P., Agbossou, E., et al., 2018. AMMA-CATCH, a critical zone observatory in west Africa monitoring a region in transition. Vadose Zone J. 17 (1), 1–24.

Goutorbe, J.P., Lebel, T., Tinga, A., Bessemoulin, P., Brouwer, J., Dolman, A.J., Engman, E.T., Gash, J.H.C., Hoepffner, M., Kabat, P., 1994. HAPEX-Sahel: a large-scale study of land-atmosphere interactions in the semi-arid tropics. In: Annales Geophysicae, vol. 12, pp. 53–64.

Guyot, A., Cohard, J.M., Anquetin, S., Galle, S., 2012. Long-term observations of turbulent fluxes over heterogeneous vegetation using scintillometry and additional observations: A contribution to AMMA under Sudano-Sahelian climate. Agricult. Forest. Meterol. 154, 84–98.

Hanan, N., Lehmann, C., 2010. Tree-grass interactions in savannas: paradigms, contradictions, and conceptual models. In: Hill, M., Hanan, N. (Eds.), Ecosystem Function in Savannas. CRC Press, Florida.

Harper, A.B., Powell, T., Cox, P.M., House, J., Huntingford, C., Lenton, T.M., Sitch, S., Burke, E., Chadburn, S.E., Collins, W.J., 2018. Land-use emissions play a critical role in land-based mitigation for Paris climate targets. Nat. Commun. 9 (1), 2938.

Heinzeller, D., Dieng, D., Smiatek, G., Olusegun, C., Klein, C., Hamann, I., Salack, S., Bliefernicht, J., Kunstmann, H., 2018. The WASCAL high-resolution regional climate simulation ensemble for West Africa: concept, dissemination and assessment. Earth Syst. Sci. Data 10 (2), 815–835.

Højstrup, J., 1981. A simple model for the adjustment of velocity spectra in unstable conditions downstream of an abrupt change in roughness and heat flux. Bound.-Layer Meteorol. 21 (3), 341–356.

Hounsinou, M., Mamadou, O., Wudba, M., Kounouhewa, B., Cohard, J.-M., 2022. Integral turbulence characteristics over a clear woodland forest in northern Benin (West Africa). Atmospheric Res. 268, 105985.

Hssaine, B.A., Ezzahar, J., Jarlan, L., Merlin, O., Khabba, S., Brut, A., Er-Raki, S., Elfarkh, J., Cappelaere, B., Chehbouni, A., 2018. Combining a Two Source Energy Balance Model Driven by MODIS and MSG-SEVIRI Products with an Aggregation Approach to Estimate Turbulent Fluxes over Sparse and Heterogeneous Vegetation in Sahel Region (Niger). Remote. Sens. 10 (6), http://dx.doi.org/10.3390/rs10060974, 974–974.

Jarvis, P.G., McNaughton, K., 1986. Stomatal control of transpiration: scaling up from leaf to region. In: Advances in Ecological Research, vol. 15, Elsevier, pp. 1–49.

Jegede, O.O., Maunder, M., Okogbue, E.C., Foken, T., Balogun, E.E., Adedokun, J.A., Oladiran, E.O., Omotosho, J.A., Balogun, A.A., Oladosu, O.R., 2004. The Nigerian micrometeorological experiment (NIMEX-1): an overview. Ife J. Sci. 6 (2), 191–202.

Jung, G., Kunstmann, H., 2007. High-resolution regional climate modeling for the Volta region of West Africa. J. Geophys. Res.: Atmospheres 112 (D23).

Kahan, D.S., Xue, Y., Allen, S.J., 2006. The impact of vegetation and soil parameters in simulations of surface energy and water balance in the semi-arid Sahel: A case study using SEBEX and HAPEX-Sahel data. J. Hydrol. 320 (1–2), 238–259.

Kljun, N., Calanca, P., Rotach, M.W., Schmid, H.-P., 2015. A simple two-dimensional parameterisation for Flux Footprint Prediction (FFP). Geosci. Model. Dev. 8 (11), 3695–3713. http://dx.doi.org/10.5194/gmd-8-3695-2015.

Knauer, J., El-Madany, T.S., Zaehle, S., Migliavacca, M., 2018. Bigleaf-An R package for the calculation of physical and physiological ecosystem properties from eddy covariance data.. PLOS ONE 13, http://dx.doi.org/10.1371/JOURNAL.PONE.0201114.

Knauer, K., Gessner, U., Fensholt, R., Kuenzer, C., 2016. An ESTARFM fusion framework for the generation of large-scale time series in cloud-prone and heterogeneous landscapes. Remote. Sens. 8 (5), 425.

Koster, R.D., Dirmeyer, P.A., Guo, Z.-C., Bonan, G., Chan, E., Cox, P., Gordon, T.C., Kanae, S., Kowalczyk, E., Lawrence, D., 2004. "Hot Spots" of Land Atmosphere Coupling.

Koster, R.D., Sud, Y.C., Guo, Z., Dirmeyer, P.A., Bonan, G., Oleson, K.W., Chan, E., Verseghy, D., Cox, P., Davies, H., 2006. GLACE: the global land-atmosphere coupling experiment. Part I: overview. J. Hydrometeorol. 7 (4), 590–610.

Lan, C., Mauder, M., Stagakis, S., Loubet, B., D'onofrio, C., Metzger, S., Durden, D., Herig-Coimbra, P.-H., 2024. Intercomparison of eddy-covariance software for urban tall-tower sites. Atmospheric Meas. Tech. 17 (9), 2649–2669.

Lebel, T., Cappelaere, B., Galle, S., Hanan, N., Kergoat, L., Levis, S., Vieux, B., Descroix, L., Gosset, M., Mougin, E., et al., 2009. AMMA-CATCH studies in the sahelian region of West-Africa: An overview. J. Hydrol. 375 (1–2), 3–13.

Linstädter, A., 2009. Landscape Ecology of Savannas. In: Bubenzer, O., Bollig, M. (Eds.), African Landscapes: Interdisciplinary Approaches. Springer New York, New York, NY, pp. 79–103. http://dx.doi.org/10.1007/978-0-387-78682-7_3.

Liu, H., Tu, G., Fu, C., Shi, L., 2008. Three-year variations of water, energy and CO 2 fluxes of cropland and degraded grassland surfaces in a semi-arid area of Northeastern China. Adv. Atmospheric Sci. 25, 1009–1020.

Lorenz, C., Kunstmann, H., 2012. The hydrological cycle in three state-of-the-art reanalyses: Intercomparison and performance analysis. J. Hydrometeorol. 13 (5), 1397–1420.

Lothon, M., Saïd, F., Lohou, F., Campistron, B., et al., 2008. Observation of the diurnal cycle in the low troposphere of West Africa. Mon. Weather. Rev. 136 (9), 3477–3500.

Mamadou, O., Cohard, J.M., Galle, S., Awanou, C.N., Diedhiou, A., Kounouhéwa, B., Peugeot, C., 2014. Energy fluxes and surface characteristics over a cultivated area in Benin: daily and seasonal dynamics. Hydrol. Earth Syst. Sci. 18 (3), 893–914. http://dx.doi.org/10.5194/hess-18-893-2014.

Mamadou, O., Galle, S., Cohard, J.M., Peugeot, C., Kounouhewa, B., Biron, R., Hector, B., Zannou, A.B., 2016. Dynamics of water vapor and energy exchanges above two contrasting Sudanian climate ecosystems in Northern Benin (West Africa). J. Geophys. Res.: Atmospheres 121 (19), 11–269.

Mauder, M., Cuntz, M., Drüe, C., Graf, A., Rebmann, C., Schmid, H.P., Schmidt, M., Steinbrecher, R., 2013. A strategy for quality and uncertainty assessment of long-term eddy-covariance measurements. Agricult. Forest. Meterol. 169, 122–135.

Mauder, M., Foken, T., 2011. Documentation and instruction manual of the eddy-covariance software package TK3.

Mauder, M., Foken, T., 2015. Documentation and instruction manual of the eddy-covariance software package TK3 (update).

Mayr, M.J., Samimi, C., 2015. Comparing the dry season in-situ leaf area index (LAI) derived from high-resolution RapidEye imagery with MODIS LAI in a Namibian Savanna. Remote. Sens. 7 (4), 4834–4857.

Merk, F., Schaffhauser, T., Anwar, F., Tuo, Y., Cohard, J.M., Disse, M., 2024. The Significance of the Leaf-Area-Index on the Evapotranspiration Estimation in SWAT-T for Characteristic Land Cover Types of Western Africa. Hydrol. Earth Syst. Sci. Discuss. 2024, 1–37.

Moore, C., 1986. Frequency response corrections for eddy correlation systems. Bound.-Layer Meteorol. 37 (1), 17–35.

Mortey, E.M., Annor, T., Arnault, J., Inoussa, M.M., Madougou, S., Kunstmann, H., Nyantakyi, E.K., 2023. Interactions between Climate and Land Cover Change over West Africa. Land 12 (2), http://dx.doi.org/10.3390/land12020355, 355–355.

Myneni, R., Knyazikhin, Y., Park, T., 2015. MOD15A2H MODIS/Terra Leaf Area Index/FPAR 8-Day L4 Global 500 m SIN Grid V006.

Nadolski, L., Bliefernicht, J., Petrovic, D., Rauch, M., Sy, S., Guug, S., Steinbrecher, R., Neidl, F., Hingerl, L., Kunstmann, H., 2024. Exploring and closing the energy balance of eddy covariance measurements along a land use gradient in the West African Sudanian savanna. Front. Water http://dx.doi.org/10.3389/frwa.2024.1393884.

Ndiaye, M.B., Sine, B., Sambakhe, D., Diallo, A.O., Muller, B., Sene, M., Sambou, S., 2024. Characterization of the starting conditions of the rainy season in Senegal: highlighting the constraints of crop establishment. Environ. Res. Commun. 6 (7), 075024.

Neupane, R.P., Kumar, S., 2015. Estimating the effects of potential climate and land use changes on hydrologic processes of a large agriculture dominated watershed. J. Hydrol. 529, 418–429.

Paulus, S.J., Orth, R., Lee, S.C., Hildebrandt, A., Jung, M., Nelson, J.A., El-Madany, T.S., Carrara, A., Moreno, G., Mauder, M., Groh, J., Graf, A., Reichstein, M., Migliavacca, M., 2024. Interpretability of negative latent heat fluxes from eddy covariance measurements in dry conditions. Biogeosciences 21 (8), 2051–2085. http://dx.doi.org/10.5194/bg-21-2051-2024, URL https://bg.copernicus.org/articles/21/2051/2024/.

Penman, H.L., 1948. Natural evaporation from open water, bare soil and grass. Proc. R. Soc. Lond. Ser. A. Mathematical Phys. Sci. 193 (1032), 120–145.

Potapov, P., Turubanova, S., Hansen, M.C., Tyukavina, A., Zalles, V., Khan, A., Song, X.P., Pickens, A., Shen, Q., Cortez, J., 2022. Global maps of cropland extent and change show accelerated cropland expansion in the twenty-first century. Nat. Food 3 (1), 19–28.

Quansah, E., Mauder, M., Balogun, A.A., Amekudzi, L.K., Hingerl, L., Bliefernicht, J., Kunstmann, H., 2015. Carbon dioxide fluxes from contrasting ecosystems in the Sudanian Savanna in West Africa. Carbon Balance Manag. 10, 1–17.

Rahimi, J., Ago, E.E., Ayantunde, A., Berger, S., Bogaert, J., Butterbach-Bahl, K., Cappelaere, B., Demarty, J., Diouf, A.A., Falk, U., 2021. Modelling gas exchange and biomass production in west african sahelian and sudanian ecological zones. Geosci. Model. Dev. Discuss. 2021, 1–39.

Restrepo-Coupe, N., da Rocha, H.R., Hutyra, L.R., da Araujo, A.C., Borma, L.S., Christoffersen, B., Cabral, O.M., de Camargo, P.B., Cardoso, F.L., da Costa, A.C.L., 2013. What drives the seasonality of photosynthesis across the Amazon basin? A cross-site analysis of eddy flux tower measurements from the Brasil flux network. Agric. For. Meteorol. 182, 128–144.

Röll, A., Niu, F., Meijide, A., Ahongshangbam, J., Ehbrecht, M., Guillaume, T., Gunawan, D., Hardanto, A., Hertel, D., Kotowska, M., et al., 2019. Transpiration on the rebound in lowland Sumatra. Agricult. Forest. Meterol. 274, 160–171.

Salack, S., Bossa, A., Bliefernicht, J., Berger, S., Yira, Y., Sanoussi, K.A., Guug, S., Heinzeller, D., Avocanh, A.S., Hamadou, B., 2019. Designing transnational hydroclimatological observation networks and data sharing policies in West Africa.

Samain, O., Kergoat, L., Hiernaux, P., Guichard, F., Mougin, E., Timouk, F., Lavenu, F., 2008. Analysis of the in situ and MODIS albedo variability at multiple timescales in the Sahel. J. Geophys. Res.: Atmospheres 113 (D14).

Seneviratne, S.I., Corti, T., Davin, E.L., Hirschi, M., Jaeger, E.B., Lehner, I., Orlowsky, B., Teuling, A.J., 2010. Investigating soil moisture–climate interactions in a changing climate: A review. Earth-Sci. Rev. 99 (3–4), 125–161.

Snyder, P.K., Delire, C., Foley, J.A., 2004. Evaluating the influence of different vegetation biomes on the global climate. Clim. Dyn. 23, 279–302.

Soltani, M., Mauder, M., Laux, P., Kunstmann, H., 2018. Turbulent flux variability and energy balance closure in the TERENO prealpine observatory: a hydrometeorological data analysis. Theor. Appl. Climatol. 133 (3), 937–956.

Spank, U., KöSTNER, B., Moderow, U., GRüNwALD, T., Bernhofer, C., 2016. Surface conductance of five different crops based on 10 years of eddy-covariance measurements.

Späth, F., Rajtschan, V., Weber, T.K.D., Morandage, S., Lange, D., Abbas, S.S., Behrendt, A., Ingwersen, J., Streck, T., Wulfmeyer, V., 2023. The land-atmosphere feedback observatory: a new observational approach for characterizing land-atmosphere feedback. Geosci. Instrum. Methods Data Syst. 12 (1), 25–44. http://dx.doi.org/10.5194/gi-12-25-2023.

Stull, R.B., 2012. An Introduction to Boundary Layer Meteorology, vol. 13, Springer Science & Business Media.

Sultan, B., Janicot, S., 2003. The West African monsoon dynamics. Part II: The “preonset” and “onset” of the summer monsoon. J. Clim. 16 (21), 3407–3427.

Sun, J., Yang, K., Yu, Y., Lu, H., Lin, Y., 2023. Land-atmosphere interactions partially offset the accelerated Tibetan plateau water cycle through dynamical processes. J. Clim. 36 (11), 3867–3880.

Sy, S., de Noblet-Ducoudré, N., Quesada, B., Sy, I., Dieye, A.M., Gaye, A.T., Sultan, B., 2017. Land-surface characteristics and climate in West Africa: Models’ biases and impacts of historical anthropogenically-induced deforestation. Sustain. 9 (10), 1917.

Sy, S., Quesada, B., 2020. Anthropogenic land cover change impact on climate extremes during the 21st century. Environ. Res. Lett. 15 (3), 034002. http://dx.doi.org/10.1088/1748-9326/ab702c.

Thom, A.., 1972. Momentum, mass and heat exchange of vegetation. Q. J. R. Meteorol. Soc. 98 (415), 124–134.

Timouk, F., Kergoat, L., Mougin, É., Lloyd, C., Ceschia, E., Cohard, J.M., De Rosnay, P., Hiernaux, P., Demarez, V., Taylor, C., 2009. Response of surface energy balance to water regime and vegetation development in a Sahelian landscape. J. Hydrol. 375 (1–2), 178–189.

Verbruggen, W., Schurgers, G., Horion, S., Ardö, J., Bernardino, P.N., Cappelaere, B., Demarty, J., Fensholt, R., Kergoat, L., Sibret, T., 2020. Contrasting responses of woody and herbaceous vegetation to altered rainfall characteristics in the Sahel. Biogeosciences Discuss. 2020, 1–26.

Wallace, J.S., Wright, I.R., Stewart, J.B., Holwill, C.J., 1991. The Sahelian Energy Balance Experiment (SEBEX): Ground based measurements and their potential for spatial extrapolation using satellite data. Adv. Space Res. 11 (3), 131–141.

Waller, M.P., Street-Perrott, F.A., Wang, H., 2007. Holocene vegetation history of the Sahel: pollen, sedimentological and geochemical data from Jikariya Lake, north-eastern Nigeria. J. Biogeogr. 34 (9), 1575–1590.

Widmoser, P., Wohlfahrt, G., 2018. Attributing the energy imbalance by concurrent lysimeter and eddy covariance evapotranspiration measurements. Agricult. Forest. Meterol. 263, 287–291.

Wulfmeyer, V., Branch, O., Warrach-Sagi, K., Bauer, H.-S., Schwitalla, T., Becker, K., 2014. The impact of plantations on weather and climate in coastal desert regions. J. Appl. Meteorol. Clim. 53 (5), 1143–1169.

Wutzler, T., Lucas-Moffat, A., Migliavacca, M., Knauer, J., Sickel, K., Šigut, L., Menzer, O., Reichstein, M., 2018. Basic and extensible post-processing of eddy covariance flux data with REddyProc. Biogeosciences 15 (16), 5015–5030.

Xue, Y., 2017. Impact of Land–Atmosphere Interactions on Sahel Climate. Oxf. Res. Encycl. Clim. Sci. http://dx.doi.org/10.1093/acrefore/9780190228620.013.514.

Xue, Y., Boone, A., Taylor, C.M., 2012. Review of Recent Developments and the Future Prospective in West African Atmosphere/Land Interaction Studies. Int. J. Geophys. 2012, 1–12. http://dx.doi.org/10.1155/2012/748921.